Research

Octopaminergic neurons have multiple targets in *Drosophila* larval mushroom body calyx and can modulate behavioral odor discrimination

J.Y. Hilary Wong,[1] Bo Angela Wan,[1] Tom Bland, Marcella Montagnese, Alex D. McLachlan, Cahir J. O'Kane, Shuo Wei Zhang, and Liria M. Masuda-Nakagawa

Department of Genetics, University of Cambridge, Cambridge CB2 3EH, United Kingdom

Discrimination of sensory signals is essential for an organism to form and retrieve memories of relevance in a given behavioral context. Sensory representations are modified dynamically by changes in behavioral state, facilitating context-dependent selection of behavior, through signals carried by noradrenergic input in mammals, or octopamine (OA) in insects. To understand the circuit mechanisms of this signaling, we characterized the function of two OA neurons, sVUMl neurons, that originate in the subesophageal zone (SEZ) and target the input region of the memory center, the mushroom body (MB) calyx, in larval *Drosophila*. We found that sVUMl neurons target multiple neurons, including olfactory projection neurons (PNs), the inhibitory neuron APL, and a pair of extrinsic output neurons, but relatively few mushroom body intrinsic neurons, Kenyon cells. PN terminals carried the OA receptor Oamb, a *Drosophila* αl-adrenergic receptor ortholog. Using an odor discrimination learning paradigm, we showed that optogenetic activation of OA neurons compromised discrimination of similar odors but not learning ability. Our results suggest that sVUMl neurons modify odor representations via multiple extrinsic inputs at the sensory input area to the MB olfactory learning circuit.

[Supplemental material is available for this article.]

Behavioral choices depend on discrimination among "sensory objects," which are neural representations of multiple coincident sensory inputs, across a range of sensory modalities. For example, "odor objects" (Gottfried 2009; Wilson and Sullivan 2011; Gire et al. 2013) are represented in sparse ensembles of neurons, that are coincidence detectors of multiple parallel inputs from odor quality channels. This principle is used widely in animals, including in mushroom bodies (MBs), the insect center for associative memory (Masuda-Nakagawa et al. 2005; Honegger et al. 2011), and in the piriform cortex (PCx) of mammals (Stettler and Axel 2009; Davison and Ehlers 2011).

The selectivity of sensory representations can be modulated dynamically by changes in behavioral state, allowing an animal to learn and respond according to perceptual task. In mammals, the noradrenergic system originating in the locus coeruleus (LC) is implicated in signaling behavioral states such as attention, arousal and expectation (Aston-Jones and Cohen 2005; Sara and Bouret 2012).

In insects, octopamine (OA), structurally and functionally similar to noradrenalin (NA) in mammals (Roeder 2005), can mediate changes in behavioral state that often promote activity; for example, sensitization of reflex actions in locusts (Sombati and Hoyle 1984), aggressive state in crickets (Stevenson et al. 2005), initiation and maintenance of flight state (Brembs et al. 2007; Suver et al. 2012), and enhanced excitability of *Drosophila* motion detection neurons during flight (Strother et al. 2018). Another role of OA is as a reward signal: A single OA neuron, VUMmx1, mediates the reinforcing function of unconditioned stimulus in the honeybee proboscis extension reflex (Hammer 1993; Hammer and Menzel 1998; Menzel 2012). In *Drosophila,* acquisition of appetitive memory is impaired in *TβH* mutants, unable to synthesize OA (Schwaerzel et al. 2003), and activation of OA neurons can substitute reinforcing stimulus in appetitive learning (Schroll et al. 2006). Moreover, OA receptors are necessary for reward learning in *Drosophila* (Burke et al. 2012) and crickets (Matsumoto et al. 2015).

To understand the neural mechanisms of OA in higher order sensory discrimination, we used the simple sensory "cortex" of larval *Drosophila*, the calyx, which is the sensory input region of the mushroom bodies (MBs), the insect memory center. Here, each MB neuron (Kenyon cell [KC]) typically arborizes in several glomeruli, most of which are organized around the terminus of an olfactory projection neuron (PN); KCs thus combinatorially integrate multiple sensory input channels (Masuda-Nakagawa et al. 2005) and are coincidence detectors of multiple inputs. The APL provides inhibitory feedback (Lin et al. 2014; Masuda-Nakagawa et al. 2014) and helps to maintain KC sparse responses and odor selectivity (Honegger et al. 2011), analogous to inhibition in the mammalian PCx (Poo and Isaacson 2009; Stettler and Axel 2009; Gire et al. 2013). Thus, odors are represented as a sparse ensemble of KCs that are highly odor selective, a property beneficial for memory (Olshausen and Field 2004).

In addition, the larval MB calyx is innervated by two OA neurons, sVUMmd1 and sVUMmx1, ventral unpaired medial neurons with dendritic fields originating in the mandibular and maxillary neuromeres, respectively, of the SEZ in the third instar larva

[1]**These authors contributed equally to this work.**
Corresponding author: lm546@gen.cam.ac.uk
Article is online at http://www.learnmem.org/cgi/doi/10.1101/lm.052159.120.

(Selcho et al. 2014). sVUMmd1 and sVUMmx1 are named as OANa-1 and OANa-2, respectively, in the EM connectomic analysis of a 6-h first instar larva (Eichler et al. 2017; Supplemental Fig. 3 of Saumweber et al. 2018). These sVUM1 neurons also innervate the first olfactory neuropile of the antennal lobe (AL). This pattern of innervation is conserved in other insects, for example, the dorsal unpaired median (DUM) neurons in locusts (for review, see Bräunig and Pflüger 2001), the VUMmx1 neuron in honeybees (Hammer 1993; Schröter et al. 2007), and OA-VUMa2 neurons in adult *Drosophila* (Busch et al. 2009). In adult *Drosophila*, OA-VUMa2 neurons also show a dense innervation of the lateral horn, implicated in innate behaviors (Busch et al. 2009). The widespread innervation of the insect olfactory neuropiles also resembles the widespread NA innervation of mammalian olfactory processing areas, such as the olfactory bulb, and piriform cortex, by LC neurons originating in the brainstem.

We characterized the innervation pattern and synaptic targets of sVUM1 neurons in the calyx, with MB intrinsic and also extrinsic neurons, the localization of the OA receptor Oamb in the calyx circuit, and the impact of sVUM1 neuron activation on behavioral odor discrimination. For this we used an appetitive conditioning paradigm, and tested the ability of larvae to discriminate between similar odors, as opposed to dissimilar odors. Since the larval connectome is based on a single brain, at first instar stage before octopaminergic connections have become as extensive as at third instar, and to obtain a comprehensive understanding of the synaptic targets of sVUM1s in the third-instar larval calyx, we extended our analysis to previously unanalyzed connectivity of VUM1s, to APL and PNs. Further, we combined light microscopy of third-instar larvae with the connectome described by Eichler et al. (2017).

We find that sVUM1 neurons in third-instar larvae contact all the major classes of calyx neuron to some degree, consistent with EM synaptic analysis of the 6-h larva (Eichler et al. 2017). A GFP fusion of the OA receptor Oamb is localized in the terminals of PNs, and activating a subset of five SEZ neurons, including sVUM1 neurons, can affect discrimination of similar odors, without affecting underlying olfactory learning and memory ability. We suggest a broad modulatory effect of sVUM1 neurons in the calyx, including a potential role in modulating PN input at the second synapse in the olfactory pathway.

Results

sVUMI neurons in the third-instar calyx and their polarity

Two OA neurons innervate throughout the calyx without obvious regional preference

At the third-instar stage, the larval calyx is innervated by two classes of OA neurons, sVUMmd1 and sVUMmx1, originating from the mandibular and maxillary neuromeres, respectively, in the subesophageal zone (SEZ), and labeled by the *Tdc2-GAL4* line (Selcho et al. 2014). These neurons are named OANa-1 and OANa-2, respectively, in the 6-h larval brain EM connectomic analysis, described by Eichler et al. (2017). OAN-a1 corresponds to VUMmd1, and OAN-a2 to VUMmx1, judging from the respective anterior and posterior positions of their cell bodies in Extended Figure 5 of Eichler et al. (2017). Both neurons are labeled by *GMR34A11-GAL4* (Supplemental Fig. 3 of Saumweber et al. 2018), which we used below in our behavior analysis. To visualize the innervation pattern of these neurons together in the more mature third-instar larva, we used the Multicolor FlpOut technique (Nern et al. 2015). Flies of genotype *pBPhsFlp2::PEST(attP3); HA_V5_FLAG_OLLAS* were crossed to flies of *Tdc2-Gal4*, and single cell clones were generated by heat shock. Each sVUM1 neuron ramified throughout the calyx, and we only ever found a single sVUMmd1 or sVUMmx1 neuron labeled. When both sVUM1 neurons were labeled, they ramified through the calyx in a nonoverlapping pattern; no fasciculation between the processes of the two neurons was observed, and each innervated the whole calyx without obvious regional preference, as shown in the 3D image (Fig. 1A). Two cell bodies were labeled in the same channel in the mandibular neuromere, but only one innervated the calyx. A single sVUM1 neuron was identifiable by labeling in a single channel in the maxillary neuromere (Fig. 1B).

Cell bodies of sVUM1 neurons are at the midline of the CNS in the SEZ; their primary processes project dorsally and bifurcate just before the esophagus foramen, to generate two laterally oriented

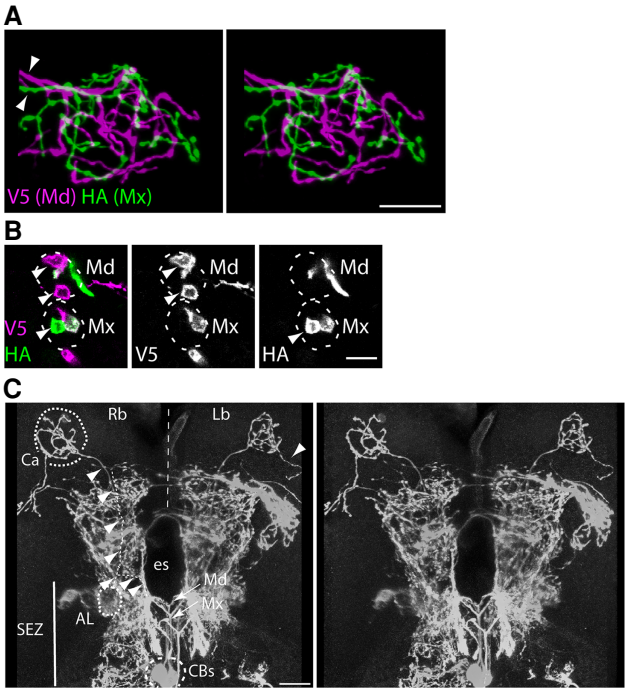

Figure 1. Multicolor FlpOut of *Tdc2-GAL4*-expressing neurons labels two calyx-innervating neurons in third-instar larvae. (*A*–*C*) Clones of larvae of genotype *w, pBPhsFlp2::PEST; Tdc2-GAL4; UAS-Ollas (attP2) UAS-HA-UAS-V5-UAS-FLAG (attP1),* were generated by heat shock induction of FLP, and identified by multicolor labeling. (*A*) 3D stereo pair of images of an sVUM1Md neuron (V5 tag) and an sVUM1Mx neuron (green, HA tag), both ramifying throughout the calyx. Arrowheads show the axons of the two neurons. Scale bar, 10 µm. (*B*) Cell bodies in the SEZ of the same larva. In the mandibular (*top*) neuromere, two cell bodies labeled in magenta can be identified labeled by antibody to V5 (arrowheads). One of these is the sVUM1md neuron. In the maxillary (*bottom*) neuromere, a single cell body is only green, identified by anti-HA (arrowhead). (*C*) 3D stereo pair of images of a frontal view of a larva in which neurons are clonally labeled with anti-V5, for anatomical clarification. An sVUM1 neuron trajectory is shown. Cell bodies (CBs) of sVUM1 neurons are at the ventral midline of the subesophageal zone (SEZ). Each sVUM1 neuron sends a primary process that bifurcates into secondary processes at the level of the mandibular (Md, arrow) for sVUM1Md, and maxillary (Mx, arrow) neuromere for sVUM1Mx. Each secondary process joins an ascending tract on each side of the esophagus foramen (es) to innervate the ipsilateral protocerebrum, right brain (Rb), or left brain (Lb). While one branch innervates the AL (antennal lobe), another branch separates to follow a tract to the calyx (Ca). Ca and AL are indicated by dotted lines. The AL can be appreciated at the ventral-anterior region of the brain in the 3D. An arrowhead shows a ventral protrusion from the calyx. The trajectories of the VUM neurons are labeled by arrowheads and smaller dotted lines. Scale bars: *A*,*B*, 15 µm; *C*, 20 µm.

secondary processes, each of which joins an ascending tract to the protocerebrum on each brain hemisphere. At the posterior of the AL, the process generates a branch that goes anteriorly and ramifies in the AL. The main branch ascends through the inner antennocerebral tract to reach the calyx at the dorsal protocerebrum. One branch emanates from the calyx and projects ventrally, presumably to the lateral horn (Fig. 1C).

OA neurons are presynaptic in the calyx

To visualize the polarity of the calyx-innervating sVUM1 neurons, we used *Tdc2-GAL4* to express either plasma membrane, presynaptic or dendritic markers (Fig. 2). The projections of both sVUMmd1 and sVUMmx1, when visualized by the plasma membrane marker CD4::tdTom, showed dense ramification throughout the calyx, with discrete and abundant bouton-like enlargements along the axonal process, predominantly among glomeruli and in the core of the calyx (Fig. 2A). The presynaptic nature of the *Tdc2-GAL4*-expressing calyx boutons was further supported by the localization of the presynaptic markers nSyb::GFP (Fig. 2A) and Syt::GFP (Fig. 2B), prominently between glomeruli or in the nonglomerular core of the calyx. Only a few dots are visible of the dendritic marker DenMark (Fig. 2B) in the terminals throughout the calyx. On the other hand, DenMark::mCherry is strongly localized in the SEZ region (Fig. 2C), where the postsynaptic processes of VUM neurons are localized. The DenMark::mCherry labeling includes dense arborizations of other *Tdc2-GAL4*-expressing neurons as well as of the sVUM1 neurons. The innervation of the calyx by *Tdc2* neurons can be visualized in Figure 2D.

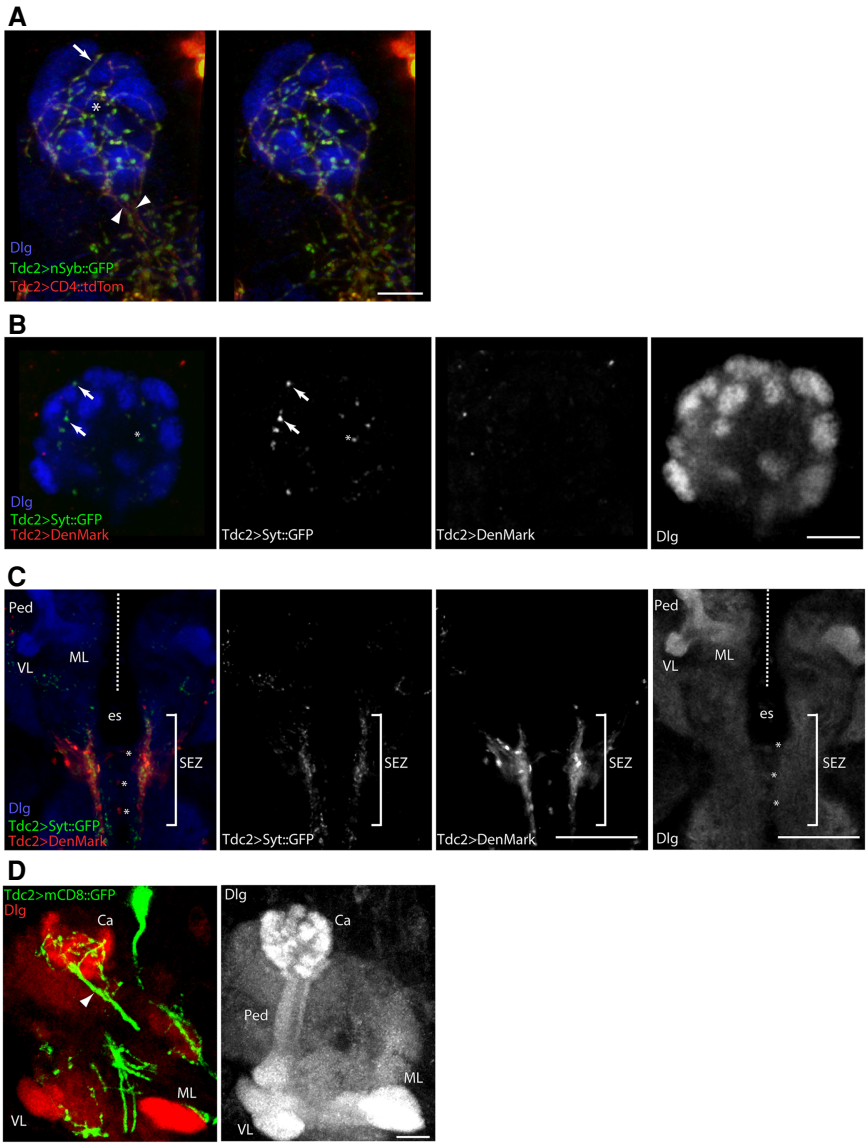

Figure 2. Polarity of calyx innervation by *Tdc2-GAL4*-expressing neurons in third-instar larvae. (*A*) 3D stereo pair of images of a third-instar calyx expressing nSyb::GFP and CD4::tdTom using *Tdc2-GAL4*, obtained from a cross between *UAS-CD4::tdTomato (II); UAS-nSyb::GFP (III)*, and *Tdc2-GAL4* parents. Two axonal tracts (arrowheads) enter the calyx and ramify throughout it (CD4::tdTom), while processes show nSyb::GFP in boutons (green). Note boutons at the borders of glomeruli (e.g., arrow; glomeruli labeled with anti-Dlg) and core of the calyx (e.g., asterisk). (*B*) Confocal section of a larval calyx expressing DenMark::mCherry and Syt::GFP using *Tdc2-GAL4*, obtained from a cross of genotype *Tdc2-GAL4* to BDSC stock 33065. Note the almost complete absence of DenMark::mCherry within the calyx. Asterisk indicates the core of the calyx with adjacent Syt::GFP puncta. Arrows indicates Syt::GFP boutons between glomeruli. (*C*) Confocal section of a larval brain expressing Syt::GFP and DenMark::mCherry using *Tdc2-GAL4*. The primary processes of *Tdc2-GAL4*-expressing neurons in the SEZ are shown (asterisks). Brain neuropiles are labeled by Dlg. (Dotted line) Midline of the CNS between right and left brain hemispheres, (es) esophagus, (VL) MB vertical lobe, (ML) MB medial lobe, (SEZ) subesophageal zone (brackets). (*D*) Frontal view of a right brain hemisphere, showing an MB calyx innervated by *Tdc2-GAL4* driving expression of mCD8::GFP. (*Left*) Projection of six sections showing the *Tdc2-GAL4* tract entering the calyx (Ca, arrowhead). (*Right*) The same projection of the MBs labeled by Dlg (right brain hemisphere). Notice the glomerular structure of the calyx. (*A*,*B*) Anterior to the bottom, medial to the right, right brain orientation. Scale bars, 10 µm. (*C*) Ventral view, anterior to the top. Scale bar, 50 µm. (*D*) Frontal view, anterior to the bottom, medial to the right, right brain. Scale bar, 10 µm.

Identifying third-instar calyx OA neuron partners

To obtain a comprehensive synaptic connectivity between sVUM1 neurons and intrinsic as well as all extrinsic neurons innervating the calyx, we used *Tdc2-LexA*, along with *GAL4* lines expressing in other calyx neurons, to drive the expression of the GFP reconstitution across synaptic partners (GRASP) (Gordon and Scott 2009) constructs *LexAop-CD4::spGFP11 and UAS-CD4::spGFP1-10* (Fig. 3). We labeled olfactory PNs using *NP225-GAL4* (Tanaka et al. 2004), and KCs using *Mef2-GAL4* (Zars et al. 2000). We also tested for GRASP between sVUM1 neurons and two other classes of extrinsic calyx neurons. First, we labeled the larval APL using *NP2361-GAL4* (Masuda-Nakagawa et al. 2014). Second, two of the "Odd" class of neurons that arborize throughout the calyx (Slater et al. 2015) have been designated MBON-a1 and MBON-a2 by Eichler et al. (2017); we identified a *GAL4* line, *OK263-GAL4*, which expresses in these neurons.

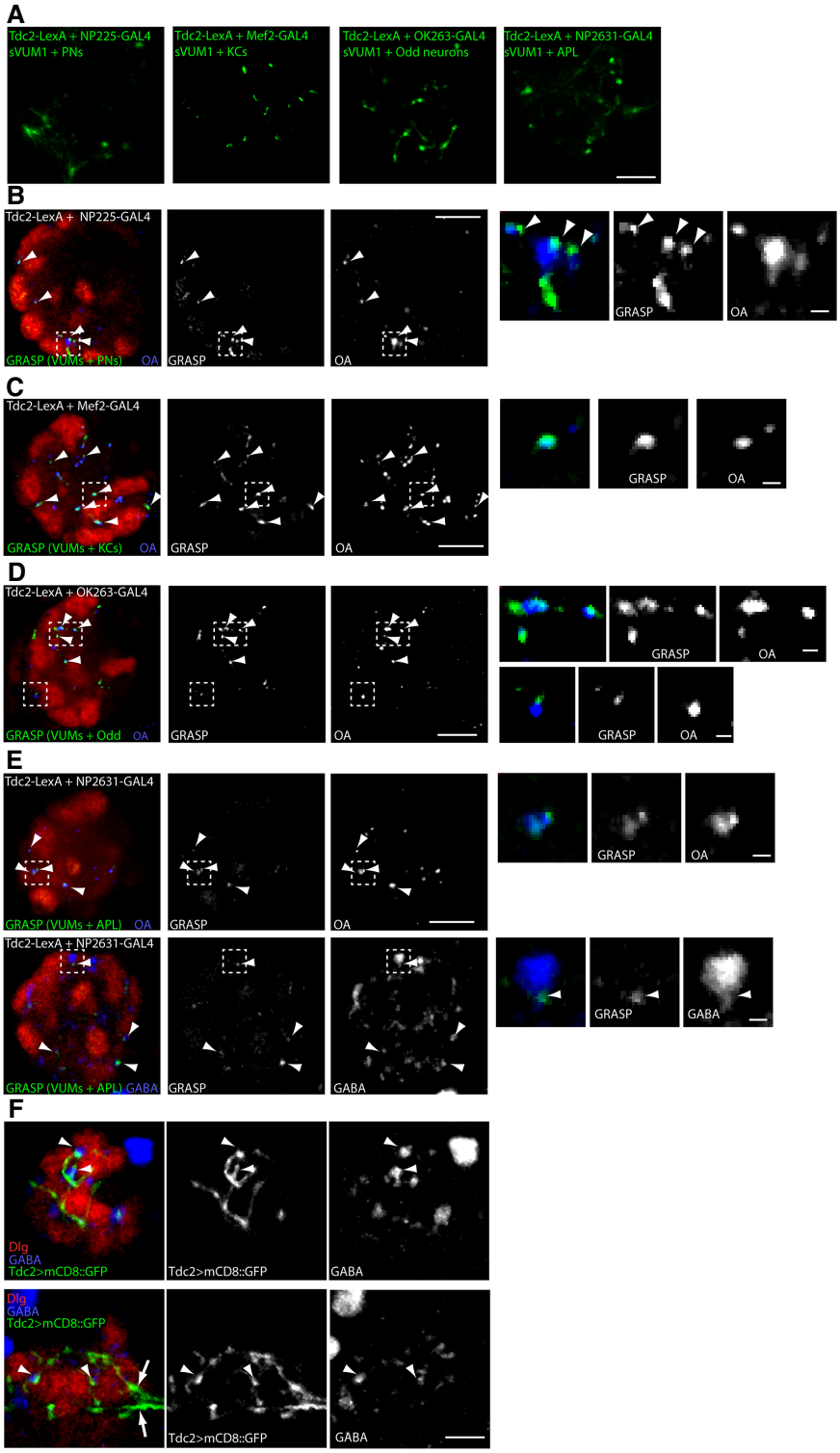

Figure 3. GRASP shows calyx contacts of sVUM1 termini with PNs, larval APL, and Odd neurons, and few KCs. A line carrying GRASP constructs *UAS-CD4::spGFP1-10* and *LexAop-CD4::spGFP11*, was crossed to each of the following lines as needed: *NP225-GAL4(II); Tdc2-LexA(III)*, *OK263-GAL4(II); Tdc2-LexA(III)*, *NP2631-GAL4(II); Tdc2-LexA(III)*, or *Tdc2-LexA(II); Mef2-GAL4(III)*, and GRASP signals were detected in the larval progeny. (*A*) GRASP signal between sVUM1 neurons (expressing *Tdc2-LexA*) and other calyx neurons expressing the *GAL4* lines shown, is detected as native GFP fluorescence in confocal sections. Scale bar, 10 µm. (*B–E*) GRASP signal between sVUM1 neurons (expressing *Tdc2-LexA*) and other calyx neurons expressing the *GAL4* lines shown, detected by rat monoclonal anti-GFP. Examples of GRASP signal are highlighted with arrowheads; areas inside broken square are shown at higher magnification. sVUM1 termini are labeled using anti-OA, calyx glomeruli using anti-Dlg. Scale bars here and throughout figure: in main panels, 10 µm; in *insets*, 1 µm. (*B*) GRASP signal between sVUM1 termini and PNs, localized mainly around glomeruli. OA signals without GRASP are localized to the calyx core. Examples of GRASP signal are highlighted with arrowheads. (*Inset*) GRASP signal overlaps partially with sVUM1 termini labeled with OA. Areas inside broken lines, here and subsequently, are shown at higher magnification. (*C–E*) GRASP signals between sVUM1 termini and KCs (*C*), Odd neurons (*D*), or the APL neuron (*E*). (*E*) GRASP signals between sVUM1 and APL neurons are localized around glomeruli, or in the core of the calyx. The *top* panels show the extent of GRASP overlap with OA-containing sVUM1 terminals. The *bottom* panels show some GRASP signals overlapping partially with large GABA boutons. (*F*) Confocal sections of a third-instar calyx expressing mCD8::GFP using *Tdc2-Gal4*, labeled with anti-GABA and anti-Dlg. *Top* is a dorsal section of calyx, *bottom* is a ventral section of the same calyx. Arrowheads indicate GABA boutons apposed to or overlapping with *Tdc2* neuron terminals. Arrows indicate the two axonal tracts of *Tdc2* neurons innervating the calyx.

GRASP fluorescence

We detected GRASP using GFP fluorescence as widely distributed puncta in the calyx, in live images of brains, suggestive of specific synaptic connections, between the sVUM1 neurons on the one hand, and PNs, KCs, the Odd, and APL neurons on the other (Fig. 3A). Control crosses expressing the GRASP constructs under control of either a *GAL4* or *LexA* calyx driver alone showed almost no GRASP puncta (Supplemental Fig. S1), showing the specificity of our rat monoclonal anti-GFP for reconstituted GFP. These findings suggest that at the third-instar larva, the sVUM1 neurons may form synapses with all the neuronal classes that innervate throughout the calyx: PNs, KCs, the APL, and Odd neurons.

To test whether GRASP signals represented synaptic contacts of the sVUM1 neurons, we also immunolabeled brains with anti-OA. GRASP signals were identified using a criterion that each GFP signal was observed in at least two consecutive confocal sections, and discounting occasional GFP-positive axonal tracts that were negative for OA. As noted below, the large majority of GFP puncta either overlapped or were directly apposed to OA signals, suggesting that GFP puncta were mostly or entirely specific for synaptic contacts, and did not form widely at nonsynaptic contacts.

OA termini synapse with PNs

Using *Tdc2-LexA* and *NP225-GAL4* to express the GRASP constructs, we found GRASP signal at 49% ± 3% of 80 ± 4 ($n = 5$) OA-positive boutons. OA-positive GRASP signals (Fig. 3B) were found in the core of the calyx away from glomeruli, in interglomerular spaces, and along the periphery of glomeruli. They are likely contacts between sVUM1 termini and PN axons. Almost all GFP puncta (87% ± 2%, $n = 5$) overlapped with or were apposed to OA boutons and are therefore potential synaptic contacts of the sVUM1 neurons; the remaining 13% could represent nonsynaptic contacts, or synapses of PNs onto postsynaptic sites on the sVUM1 neurons. Therefore, PNs are commonly postsynaptic to the termini of sVUM1 neurons, on their axonal or presynaptic processes, making axon–axon synapses.

OA termini synapse with KCs in the calyx

Using *Tdc2-LexA* and *MB247-GAL4* to express the GRASP constructs, we found GRASP signals at 51% ± 4% of 185 ± 34 ($n = 3$) OA boutons in each calyx (Fig. 3C). GRASP puncta overlapping with OA were found in the interglomerular space. Again, most GFP puncta (86% ± 1%) overlapped with or were apposed to OA. Since third-instar larvae are estimated to have 250–300 KCs per brain hemisphere (Pauls et al. 2010), our data suggest that sVUM1 neurons together synapse onto up to about one-third of third-instar KCs.

OA termini synapse with Odd neurons in the calyx

Using *Tdc2-LexA* and *OK263-GAL4* to express the GRASP constructs, we found GRASP signals at 51% ± 0.3% of 124 ± 4 ($n = 3$) OA labeled boutons (Fig. 3D). Again, the majority of GFP puncta (80% ± 1%) overlapped with or were apposed to OA, suggesting that Odd neurons are mostly postsynaptic to sVUM1s.

OA termini synapse with the APL

Using *Tdc2-LexA* and *NP2361-GAL4* to express the GRASP constructs, we found GRASP signal at 77% ± 4% of 74 ± 12 ($n = 4$) OA terminals, indicating that sVUM1 neurons are presynaptic to the larval APL (Fig. 3E top panels). Most of these GRASP signals were found between glomeruli, and more abundant toward the ventral calyx.

Around 67% ± 3% of GFP ($n = 3$) signals overlapped with OA, and therefore likely represent synapses of the sVUM1 neurons onto the APL. A higher frequency of GFP puncta did not overlap with OA (33% ± 3%) than was the case for other calyx neurons; this could potentially be due to synapses of the APL onto OA neuron axons. In support of this, we found some GABA termini in close proximity to GRASP (Fig. 3E, bottom panels); labeling of *Tdc2-GAL4 > mCD8::GFP* calyces with anti-GABA also showed some apposition of sVUM1 boutons to GABAergic termini of the APL (Fig. 3F).

Single–cell GRASP

While the above GRASP experiments reveal the partners of the sVUM1 neurons in the calyx, they do not reveal whether the sVUMmd1 and sVUMmx1 have different partners. We therefore performed single-cell GRASP to label the contacts of each sVUM1 randomly, using Brp::mCherry as a presynaptic marker to verify whether GRASP signals have a synaptic localization. We distinguished the two sVUM1 neurons by the positions of their cell bodies in the SEZ, using local neuropil landmarks revealed by anti-Dlg labeling (Fig. 4A), and using single cell clones, we could identify sVUMmd1 and sVUMmx1 individually (Fig. 4B).

GRASP signals were detected between the Odd neurons and both sVUMmd1 and sVUMmx1 (Fig. 4C), and similarly between the larval APL, and both sVUMmd1 and sVUMmx1 (Fig. 4D). Compared with standard GRASP, single cell GRASP signals were fewer, but clearly present and overlapping with the presynaptic marker Brp::mCherry (Fig. 4D). The main targets of VUMmd1 and VUMmx1 in the olfactory pathway are the antennal lobe (AL), and calyx, as described in Selcho et al. (2014). There is also a prominent branch innervating the basolateral protocerebrum (anteromedial to the AL) around the ventral midline at the esophagus foramen (as defined for adult flies, Busch et al. 2009) in the brain. Therefore, at least as judged by the APL and Odd neurons, both sVUM1 neurons appeared to have similar targets in the calyx.

Comparison with first instar larva calyx synapses

The enlargements seen using synaptic markers in Figure 2A contained OA (Fig. 3), therefore they are presynaptic boutons. Using the online publicly available first instar connectome (https ://l1em.catmaid.virtualflybrain.org) on the Virtual Fly Brain site (Osumi-Sutherland et al. 2014; Cantarelli et al. 2018), we analyzed the synapse distribution and synaptic partners of the sVUM1 neurons specifically in the first instar larva calyx, not previously analyzed. We generated a tracing representation of the sVUM1 neurons (Fig. 5A,B) using the 3D tool of the publicly available CATMAID software. While the growth, morphology, and anatomical organization of the two sVUM1 neurons is similar to the anatomical organization of the third-instar larvae, the arborizations in the calyx are fewer in the first instar compared with third-instar larvae. In our GRASP analysis, we observed 89 ± 7 (mean ± SEM; $n = 12$) OA-positive boutons per calyx for both sVUM1 neurons, compared with 28 presynaptic synapses marked in the left brain calyx, and around 39 in the right brain calyx in the single 6-h larva brain connectome (Fig 5C,D).

Moreover, the number of connections between sVUM1 and other neurons was substantially lower at the first instar compared with the third-instar stage (Supplemental Table S1), with the first-instar brain having <50% of synaptic numbers per calyx per neuron type compared with the third-instar brain.

Given the GRASP signals at sVUM1 synaptic termini, we predicted that we might find the same sVUM1 synaptic targets in the first-instar calyx connectome. Eichler et al. (2017), reported synapses of sVUM1 onto the Odd neurons, and a small fraction of

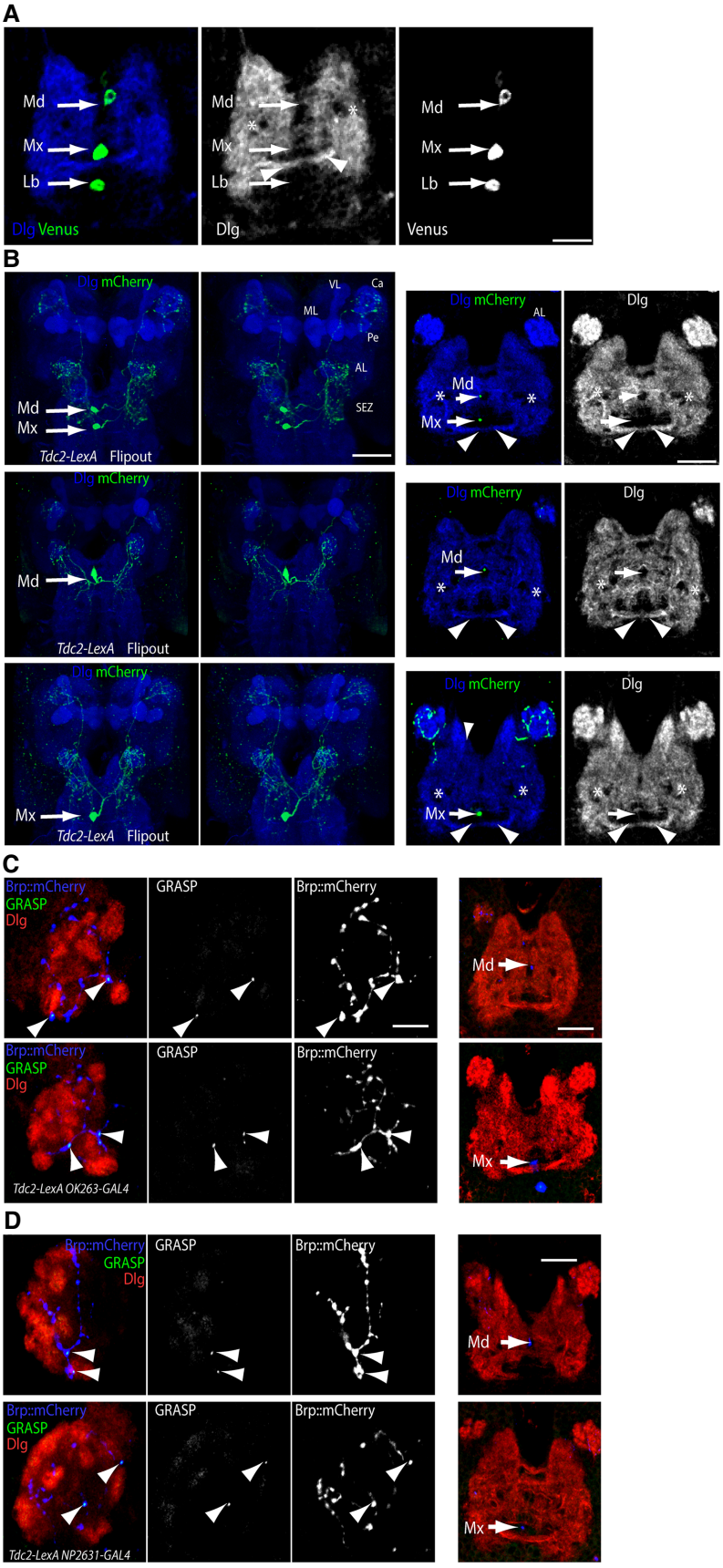

Figure 4. (Legend on next page)

KCs. We found examples of these synapses, and additionally, synapses not yet described between sVUM1 neurons onto PNs and the APL neuron (Fig. 5E). In addition to the apparently simple synapses of sVUM1 neurons onto PNs, KCs, Odd neurons, and the APL, we sometimes found adjacent synaptic contacts of either sVUM1 neuron onto both an Odd neuron and the APL (Fig. 5E), suggesting locally coordinated circuit regulation of both these neurons by the sVUM1 neurons. Clear vesicles and typical synaptic bars were present in sites of connectivity between sVUM1s and other neurons (Fig. 5E), supporting a synaptic release of octopamine. Although sVUM1s also contain dense core vesicles, our studies did not address whether sVUMs release neuropeptides.

Localization of a genomic Oamb::GFP fusion in PN terminals in calyx

To further understand how and where OA might act in the calyx, we investigated the localization of OA receptors in the calyx. *Drosophila* has a number of OA receptor classes defined both by sequence comparisons and pharmacology. Octopamine receptor in mushroom bodies (Oamb, also known as Dmoa1A or CG3856), an ortholog of human α1-adrenergic receptor (Roeder et al. 2003; Bauknecht and Jékely 2017), is enriched in the MBs (Han et al. 1998). *Drosophila* also has three OctβR receptors, which stimulate cAMP levels (Balfanz et al. 2005; Maqueira et al. 2005).

To detect the expression and subcellular localization of Oamb, we used recombinase-mediated cassette exchange (RMCE) with a MiMIC insertion (Venken et al. 2011), *MI12417*, in the third coding-region intron of *Oamb*, to tag endogenous *Oamb* with an exonic *EGFP-FlAsH-StrepII-TEV-3xFlag* fusion (Supplemental Figs. S2–S5). Insertion of an EGFP-encoding exon here should tag all known splice variants of the Oamb protein in their third cytoplasmic loop, downstream from transmembrane (TM) domain 5 (Supplemental Figs. S6, S7); this includes the alternative TM6–TM7 regions encoded by two alternative groups of C-terminal exons (Supplemental Figs. S5–S7). Therefore, a protein trap generated from the *MI12417* insertion will not disrupt any transmembrane domains.

Six recombinant *Oamb::EGFP* stocks were recovered with the EGFP-encoding exon inserted in the same orientation as the *Oamb* transcript (Supplemental Fig. 7). One of these was designated as *Mi{PT-GFSTF.1}Oamb*$^{MI12417\text{-}GFSTF.1}$, or *Oamb(MI12417)::EGFP.1* or *Oamb::EGFP*

for short. Both the original *MI12417 MiMIC* insertion, and *Oamb (MI12417)::EGFP* stocks were homozygous infertile, as expected from the egg-laying defects of *Oamb* mutants (Deady and Sun 2015), suggesting that the Oamb::EGFP fusion might not be a functional Oamb protein. However, Oamb::EGFP was localized to glomeruli in the larval calyx (Fig. 6), implying that the protein folded normally and was not degraded by the ER unfolded protein response. Expression of *UAS-RFP* in the olfactory PN line *NP225-GAL4* showed localization of Oamb::EGFP in all PN termini labeled with the GAL4 line, as well as in some calyx glomeruli not labeled by *NP225-GAL4*, which may be either sites of nonolfactory sensory input, or olfactory glomeruli not labeled by *NP225-GAL4* (Fig. 6A). The restriction of Oamb::EGFP to specific glomeruli implies that it is unlikely to be expressed in KC dendrites in the calyx, which arborize through all glomeruli. We also found no overlap of Oamb::EGFP with GABAergic APL terminals in the calyx (Fig. 6B), implying that it was not expressed in the larval APL. *OK263-GAL4* calyx projections also showed little or no overlap with Oamb::EGFP (Fig. 6C), suggesting that Oamb is not expressed in the Odd neuron calyx dendrites.

In the olfactory pathway Oamb::EGFP was detected diffusely in the AL. Cell bodies of PNs labeled by *NP225-GAL4 > mCD8::RFP* also expressed Oamb::EGFP (Fig. 6D), and other neurons surrounding the AL, but not labeled by *NP225-GAL4 > mCD8::RFP*, expressed Oamb::EGFP (Fig. 6D). These could be interneurons and potentially the main source of labeling in the AL. No distinct glomeruli were detected. Oamb::EGFP was detected in the lateral horn, along the lateral pedunculus, with strong expression toward the anterior lateral end, where a separate compartment along the pedunculus is labeled (Fig. 7A,B). Oamb::EGFP is detected around the medial lobe and the spur, spur as defined by Figure 6E of Younossi-Hartenstein et al. 2003 (Fig. 7C). This localization of Oamb::EGFP overlaps with innervation by *Tdc2-GAL4*-expressing neurons in the spur and around the ventral medial lobe (Fig. 7D).

We found no detectable localization of MiMIC GFP-tagged DmOctβR receptors to the calyx (data not shown). Octβ1R::EGFP (*CG6919*) was detected weakly in a few ventral and medial AL glomeruli by a polyclonal anti-GFP, but was not detectable in the calyx. Octβ2R::EGFP (*CG6989*), was not detectable in either the calyx or AL, although it was expressed in a number of adjacent cell bodies that did not colocalize with PNs as labeled by *NP225-GAL4* driving RFP expression. We could not detect Octβ3R::EGFP anywhere in the brain, and therefore the fusion might not be expressed, or misfold and be degraded.

Activating an OA neuron subset including sVUM1 neurons impairs behavioral odor discrimination

Since the calyx is a site where MB neurons process olfactory information that comprises conditioned stimuli in associative learning, we reasoned that modulating the processing of this information might affect the ability of the brain to discriminate among different conditioned stimuli representations while learning, but without affecting its underlying learning ability. Therefore, to test whether OA innervation of the calyx affected odor discrimination during learning, we developed an assay that could distinguish odor discrimination ability from learning ability (Fig. 8). The rationale of this assay was developed in the honeybee by Stopfer et al. (1997) in pattern recognition. Desynchronization of PN ensembles impaired fine discrimination of molecularly similar odors but not dissimilar odors. When bees are conditioned with one odor and sucrose, the conditioned response generalizes to structurally similar odors used for conditioning (Smith and Menzel 1989). Therefore, we reasoned that mixtures of two odors at different ratios would be more similar and harder to distinguish than the two pure constituent odors, and this would allow us to test changes in the degree of discrimination ability by activation of sVUM1 neurons; this rationale was used successfully by Lin et al. (2014). By combining odor choice with an appetitive learning paradigm (Scherer et al. 2003), we tested the effect on behavioral odor discrimination of optogenetic activation of OA neurons in third-instar larvae, using the long-wavelength absorbing channelrhodopsin, CsChrimson (Klapoetke et al. 2014).

Since we did not have *GAL4* or *LexA* drivers completely specific for sVUM1 neurons, we used an intersectional approach to restrict the expression of CsChrimson to a small subset of OA neurons including the sVUM1 neurons. We could use *LexAop-FLP* and a *GAL80* cassette flanked by two *FRT* sites to express *UAS-CsChrimson* only in neurons that expressed both *GMR34A11-GAL4* (which labels some VUM neurons in addition to non-OA neurons), and *Tdc2-LexA*. We thus expressed CsChrimson in only five OA neurons in the SEZ of the larval brain: two in the mandibular neuromere (including sVUMmd1), two in the maxillary neuromere (including sVUMmx1), and one in the labial neuromere ($n = 8$) (Fig. 9A). The second neuron labeled in each neuromere could be the sVUM2, characteristic for the lateral branch innervating the optic lobe; the sVUM3, which innervates the dorsal medial protocerebrum and basal medial protocerebrum (Selcho et al. 2014); or an unidentified sVUM; however, sVUM1 neurons are the only neurons of this subset to innervate the AL and calyces.

Activation of these OA neurons by amber light, during conditioning, had no effect on the ability of larvae to discriminate odors in an appetitive odor discrimination learning assay using a dissimilar odor pair; however, it abolished their ability to discriminate a similar odor pair, suggesting that odor discrimination is affected by activation of these neurons, but not underlying learning ability (Fig. 9B). To exclude any effects of OA

Figure 4. Single-cell GRASP of sVUM1 neurons in the calyx. (*A*) Identification of sVUM1 neurons based on SEZ anatomical landmarks. Males of genotype *w/Y; Tdc2-LexA(II); GMR34A11-GAL4(III)/TM6B* were crossed to females of genotype *Tub84B(FRT-GAL80)1, w; LexAop2-FLPL(II); UAS-Chrimson.mVenus(III)/TM6B*. The larval progeny of this cross, of genotype *FRT.GAL80 w/(w or Y); Tdc2-LexA(II)/LexAop2-FLPL (II); GMR34A11-GAL4(III)/UAS-CsChrimson.mVenus(III)*, express Venus in cells that express both *Tdc2-LexA* and *GMR34A11-GAL4*. sVUM1md neurons (Md) are in a small anterior medial Dlg-negative gap, with bilaterally symmetrical gaps (asterisks) nearby. sVUM1mx neurons (Mx) are localized in a large medial gap that lies just anterior to a commissural DLG pathway (arrowheads). sVUMlb neurons (Lb) are localized posteriorly to this commissural pathway. Scale bar, 24 µm. (*B–D*) Single-cell GRASP was induced between sVUM1 neurons expressing *Tdc2-LexA*, and potential calyx partner neurons that expressed different *GAL4* lines. sVUM1 neurons were individually labeled by heat-shock-induced FlipOut of larvae of genotype *P{hsFLP}12/(w or Y); GAL4(II)/+; Tdc2-LexA(III)/LexAOp2-IVS > stop > spGFP11::CD4::HA-T2A-Brp::mCherry (attP2), UAS-spGFP1-10::CD4, UAS-HRP::CD2*. (*B*) Single-cell clones, expressing Brp::mCherry in subsets of *Tdc2-LexA*-expressing neurons; each row shows a separate clone. The *left* image pairs are stereo views of reconstructions showing the entire trajectory of labeled neurons; MB calyx (Ca), pedunculus (Pe), medial and vertical lobes (ML and VL), antennal lobe (AL), and subesophageal zone (SEZ) are labeled in the *top* row. *Right* images are single confocal sections through the SEZ of the same larvae, showing the primary process of each labeled sVUM1 (arrows) and the anatomical landmarks shown in *A*. (First row) sVUMmd1 and sVUMmx1. (Second row) sVUMmd1. (Third row) sVUMmx1. Scale bars: 3D images, *left*, 45 µm; SEZ sections, *right*, 30 µm. (*C,D*) Single-cell GRASP between sVUM1 neurons expressing *Tdc2-LexA*, and Odd neurons expressing *OK263-GAL4* (*C*), or larval APL expressing *NP2631-GAL4* (*D*). (*Left* panels) Larval calyx labeled with anti-DsRed to visualize Brp::mCherry (enriched at presynaptic sites but not confined to them), anti-Dlg to label neuropile, and anti-GFP to visualize GRASP signals. Arrowheads indicate GRASP signals. (*Right* panel) Region of same brain labeled with anti-Dlg to visualize neuropile, and anti-DsRed to visualize the VUM neurons. The *top* rows show sVUMmd1 (Md), and the *bottom* rows show sVUMmx1 (Mx). Arrows indicate the primary process of each sVUM1 neuron. Scale bars, 10 µm.

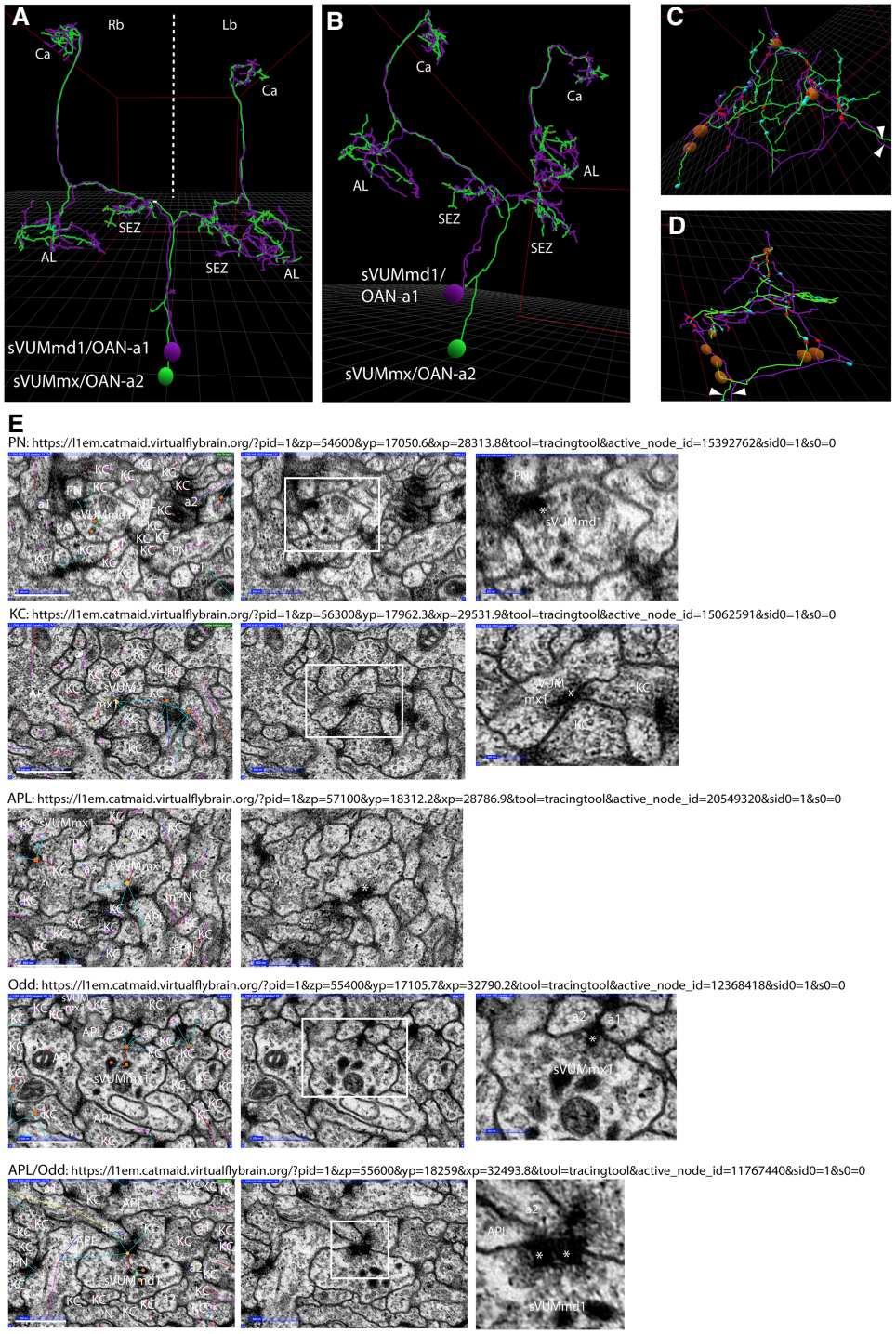

Figure 5. Synapses of sVUM1 neurons onto other first-instar calyx neurons. (*A*) Ventral view of a reconstruction of sVUMmd1/OAN-a1 (magenta) and sVUMmx1/OAN-a2 (green), including their dendritic arborizations in the subesophageal zone (SEZ) and presynaptic terminals in the antennal lobe (AL) and calyx (Ca). The right brain (Rb) is to the *left* of the midline (dotted line), and left brain (Lb) to the *right*. sVUM1 neurons bifurcate at the midline and a single neuron innervates both brain hemispheres. (*B*) A ventrolateral view of the same reconstructions as *A*. (*C*,*D*) Reconstructions of sVUM1md1 and sVUMmx1 calyx projections in the right (*C*) and left (*D*) brain. Red circles are sVUM1 presynaptic termini (blue circles are postsynaptic sites). Note the 39 presynaptic terminals of sVUM1 neurons in the right calyx (*C*) and the 28 presynaptic termini in the left calyx (*D*). Brown circles are tracing sites not finished. Images were generated by analysis of neuron tracing using the 3D tool of CATMAID on the publicly available first-instar larval connectome on the Virtual Fly Brain site (https://l1em.catmaid.virtualflybrain.org; License CC-BY-SA_4.0). (*E*) EM sections of first-instar calyx (Eichler et al. 2017) showing synaptic partners of either sVUMmd1 or sVUMmx1, named as OAN-a1 and OAN-a2 by Eichler et al. (2017) and in CATMAID as "anterior ladder" and "posterior ladder" neurons, respectively. Sections were visualized using CATMAID software via the Virtual Fly Brain site. Each row shows a different example of postsynaptic target neurons: a PN, a KC, the APL (labeled in CATMAID as MBE12), Odd neurons (MBON-a1 and MBON-a2, labeled here as a1 and a2, and in CATMAID as MBE7a and MBE7b), and a tripartite synapse of an sVUM1 neuron on both an Odd neuron (MBON-a2) and the APL. In each row, the first (*left*) panel shows a section with CATMAID annotation, and the identities of neurons close to the sVUM1 neuron and its synaptic target. Notice the connector (orange-filled circle) placed on the sVUM1 neuron and the linked cyan arrows projecting to postsynaptic partners. Red arrows pointing to the connector indicate that the connector is on the presynaptic neuron. The second panel shows the same image with annotation omitted to allow better visualization. The third panel (where present) shows a magnified view of the inset in the middle panel; a presynaptic release site in the sVUM1 neuron, characterized typically by a T-bar and surrounding synaptic vesicles, is shown with an asterisk. Scale bars, 500 nm. URLs link to the locations of images shown.

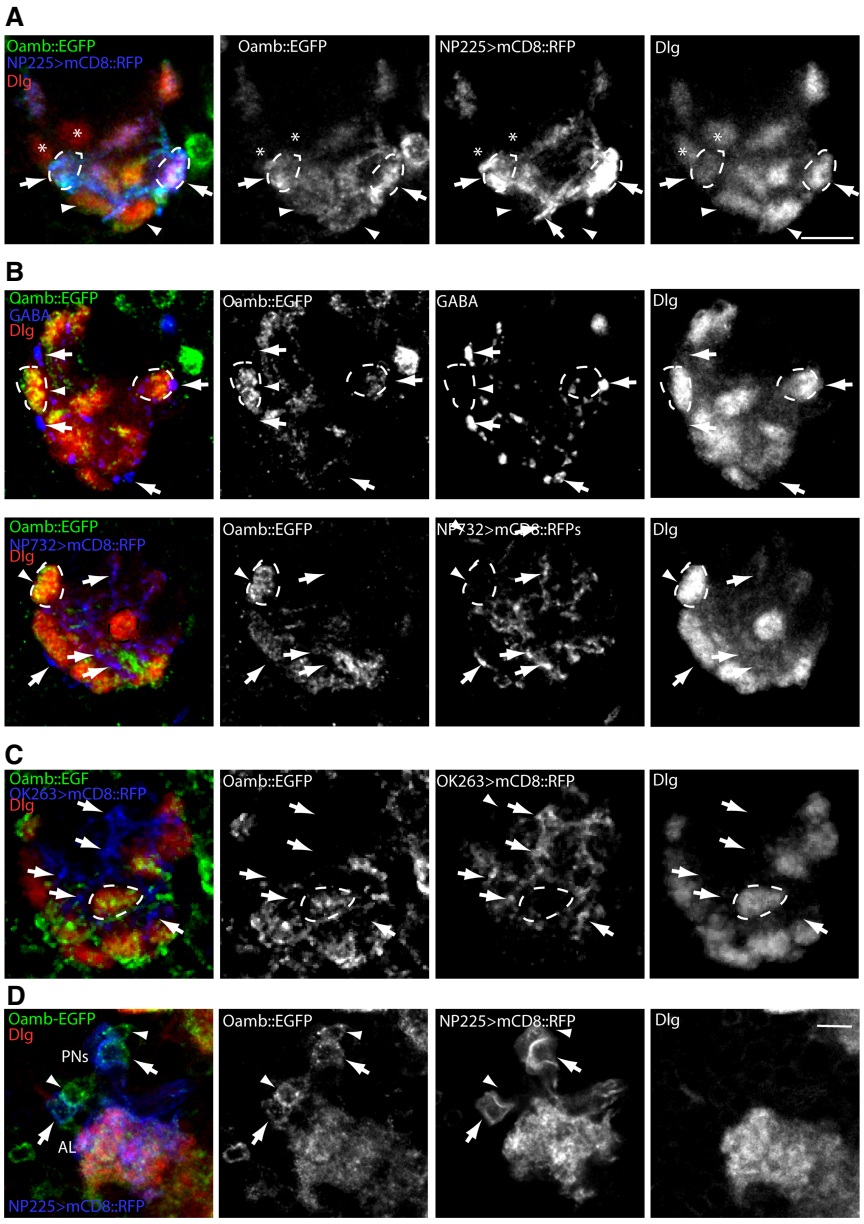

Figure 6. Oamb-EGFP localization in PN presynaptic termini. (*A*) Calyces of a larva carrying *Oamb::EGFP*, *NP225-GAL4*, and *UAS-RFP* labeled with chick polyclonal anti-GFP, anti-DsRed and anti-Dlg. Oamb::EGFP localizes to PN terminals in all glomeruli labeled by *NP225-GAL4* (arrows), and to a few glomeruli not labeled by *NP225-GAL4* (arrowheads). A few glomeruli express neither *NP225-GAL4* nor Oamb::EGFP (asterisks). One arrow indicates a PN process. (*B*, *top* row) Oamb::EGFP does not overlap with APL termini labeled by anti-GABA (example at arrows). Note the prominent GABA boutons without Oamb::EGFP at the periphery of glomeruli. (*Bottom* row) APL projections labeled by *NP0732-GAL4*. Varicosities along processes are devoid of Oamb::EGFP. (*C*) Oamb::EGFP does not overlap substantially with Odd neuron dendrites labeled by *OK263-GAL4*. Prominent varicosities are devoid of GFP (arrows). A glomerulus labeled by Oamb::EGFP does not overlap with Odd neuron dendrites (dotted line). (*A*–*C*) Representative glomeruli labeled by Oamb::EGFP are indicated by dotted lines and arrows. (*D*) Antennal lobe of a larva carrying *Oamb::EGFP*, *NP225-GAL4*, and *UAS-RFP* labeled with chick polyclonal anti-GFP, anti-DsRed, and anti-Dlg. Oamb::EGFP is detected in PN cell bodies (arrows), and cell bodies not labeled by *NP225-GAL4* (arrowheads). Notice the weak diffuse labeling of Oamb::EGFP in the AL. Scale bar, 10 µm.

activation on the unconditioned stimulus pathway during differential conditioning using the similar odor pair under amber light, we tested for an effect of amber light applied during testing, after conditioning as normal in blue light. Similar to activation during conditioning (Fig. 9B), CsChrimson activation during testing also abolished odor discrimination learning that was seen under blue light (Fig. 9C). Underlying odor preferences between the similar odor pair were also not affected by OA neuron activation, nor by the amber light used to activate them (Fig. 9D).

Discussion

OA neurons target extrinsic neurons within the calyx circuitry

Two OA neurons originating in the SEZ, sVUMmd1 and sVUMmx1, innervate the same brain neuropiles, with postsynaptic processes in the SEZ and presynaptic processes in the antennal lobe and MB calyces (Fig. 2). Using GRASP, we found contacts of sVUM1 presynaptic terminals with KCs, PNs, Odd, and APL neurons in the calyx. Most of these overlap with OA boutons, suggesting that sVUM1 terminals are mainly presynaptic, acting on presynaptic regions of PNs and the APL, and dendritic regions of KCs and the Odd neurons. Most third-instar KCs have about six dendritic processes ending in a claw around a calyx glomerulus (Masuda-Nakagawa et al. 2005), and our GRASP counts of sVUM1-KC contacts overlapping with OA are far fewer than the termini that would be needed to synapse onto the 250–300-KCs present in third-instar larvae (Pauls et al. 2010). Eichler et al. (2017) also find inputs of either sVUM1 neuron (which they call OAN-a1 and OAN-a2) into <10%–15% of KCs in first-instar larvae. Therefore, context-dependent signaling by OA in the calyx must principally affect MB activity via other MB neurons, rather than by direct action on KC dendrites, although the sVUM1 neurons may act directly on a subset of KCs.

Connectomic analysis of a 6-h first-instar larva shows that the sVUM1 neurons, OAN-a1 and OAN-a2 neurons (Eichler et al. 2017), with only 28 presynaptic termini marked in a left brain and 39 in a right brain (Fig. 5), have a qualitatively similar but less extensive calyx innervation pattern than we observe in third instar, with around 89 OA-positive boutons per calyx, and even more active zones, assuming multiple active zones per bouton. Neuromodulatory inputs might develop later in development, as they might need experience-dependent activity to develop, and when behavioral demands increase at a more mature state. Processes of sVUM1 neurons throughout the calyx were more elaborated in the third instar (Fig. 1) compared with the sparse branching of sVUM1 neurons in the first-instar larval connectome image (Fig. 5). Consistent with

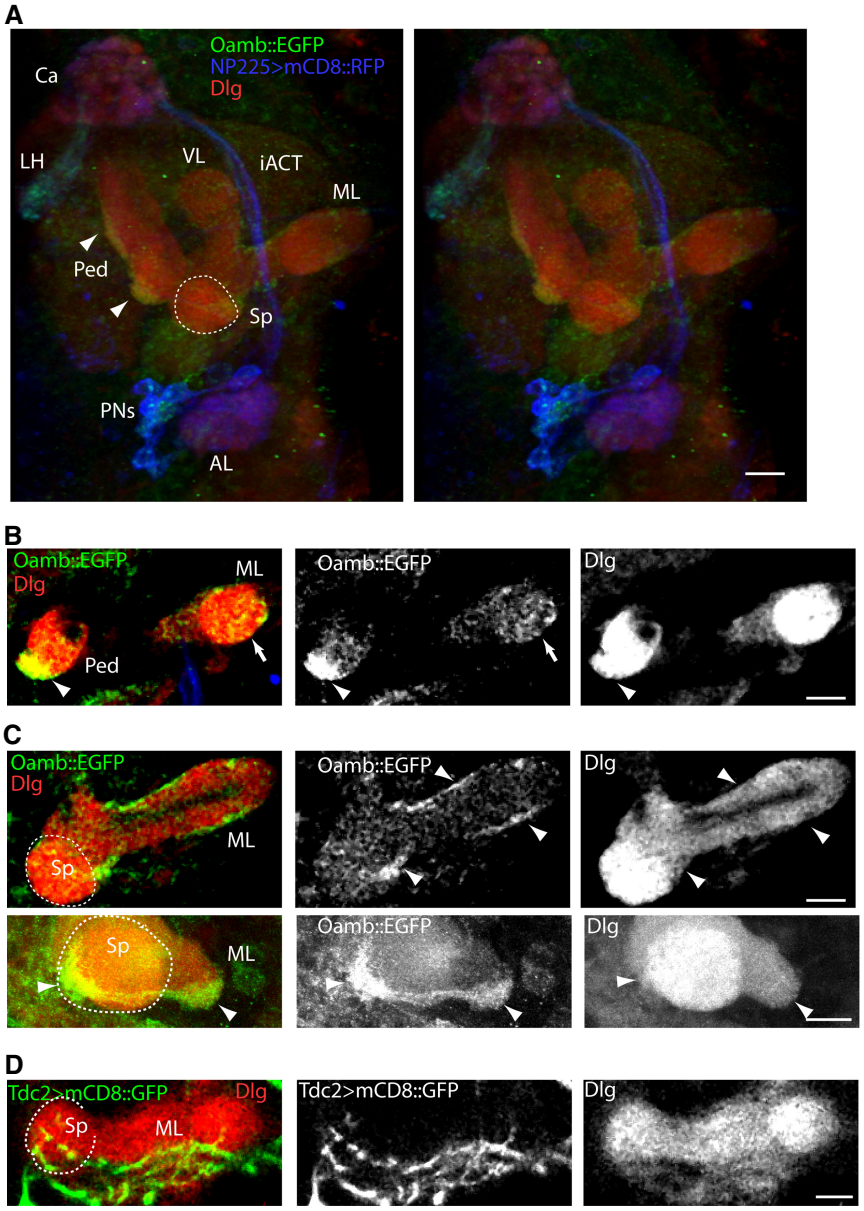

Figure 7. Oamb-EGFP localization in MB pedunculus and lobes. (*A*) 3D stereo pair of images of frontal views of a third-instar larval PN pathway in a single brain hemisphere, expressing *Oamb::EGFP*, *NP225-GAL4* and *UAS-RFP* labeled with chick anti-GFP, anti-DsRed, and anti-Dlg. PNs with cell bodies lateral to the AL project to the MB calyx and the LH (lateral horn) via the iACT (inner antennocerebral tract). Oamb::EGFP was detected at the lateral horn (LH) and calyx, lateral pedunculus (arrowheads), and medial lobes (ML). (*B*) Confocal section showing Oamb::EGFP localization in lateral pedunculus (arrowhead) and medial lobe (arrow). (*C*, *top* row) Confocal section showing Oamb::EGFP in the medial lobe (ML) and in the heel of the MB. (*Bottom* row) Higher-magnification section of Oamb::GFP labeling at the spur (Sp) and medial lobe. (*D*) Section through the MB spur and medial lobe in third-instar larva carrying *Tdc2-GAL4* and *UAS-mCD8::GFP*. Notice the GFP-expressing processes at the ventral side of the medial lobe and the spur. The spur region is indicated by dashed lines in *A*, *C*, and *D*. Scale bars, 10 µm.

our findings, Eichler et al. (2017) also report presynaptic contacts of sVUM1 neurons with Odd neuron dendrites, and some synapses of sVUM1 neurons with KCs, but not with most KCs; they do not comment on synapses with PNs or the APL.

Roles of APL and Odd neurons in calyx activity

sVUM1 presynaptic termini make many contacts with both the APL and Odd neurons in third-instar larvae (Figs. 3, 4). Odd neurons ramify throughout the calyx and receive input from PNs generally, potentially forming a channel for nonselective odor processing that is parallel to the main MB odor-specific processing through KCs. sVUM1 neurons could potentially change the Odd neuron gain or tuning properties, to signal changes in behavioral state that guide odor-driven choice behaviors, for example during chemotactic behavior, in which Odd neurons are implicated (Slater et al. 2015).

The APL mediates a negative feedback loop from KC outputs in the MB lobes to KC inputs in the calyx, thus potentially both limiting the duration of KC activity and improving their odor discrimination (Lin et al. 2014; Masuda-Nakagawa et al. 2014). sVUM1 synapses onto the APL in the calyx could therefore potentially modulate this feedback loop. This could increase signal-to-noise ratio, in a context-dependent manner, by sharpening odor representations in the calyx via APL inhibitory feedback, similar to the "gain control" mechanism with enhancement of behaviorally relevant responses and suppression of nonrelevant ones in monkey visual system (Treue and Martínez Trujillo 1999; Gilbert and Li 2013). On the other hand, at extremes, this would also decrease the sensitivity to input, and hence decrease learning. Inhibition of the APL enhances learning, by increasing the sensitivity to input (Liu and Davis 2009).

In addition, since we observed some GRASP signals adjacent to GABA termini (Fig. 3E), APL feedback could also inhibit OA release from sVUM1 termini, further increasing the complexity of interactions between OA innervation and the KC/APL negative feedback loop. NA regulation of inhibitory neurons is also a feature of the mammalian olfactory circuitry. In the olfactory bulb, disinhibition of mitral cell (equivalent to PN) activity by NA regulation of inhibitory granule cells has been proposed (Nai et al. 2009). In mammalian PCx, feedforward and feedback inhibition are postulated to enhance cortical representation of strong inputs (Stokes and Isaacson 2010), and the PCx receives extensive NA innervation from the LC, although its role in modulating inhibition has not been investigated.

PNs as potential targets of OA modulation

GRASP analyses suggest that PNs are postsynaptic to the sVUM1 neurons (Fig. 3). Indeed, an Oamb::EGFP exon-trap fusion is localized on PN presynaptic terminals, albeit more widely than GRASP puncta (Fig. 6). Similarly, the honeybee Oamb ortholog AmOA1 is found widely in the calyx (Sinakevitch et al. 2011), although these authors do not distinguish between PN terminals or KC dendrites. Much aminergic neurotransmission acts via extrasynaptic

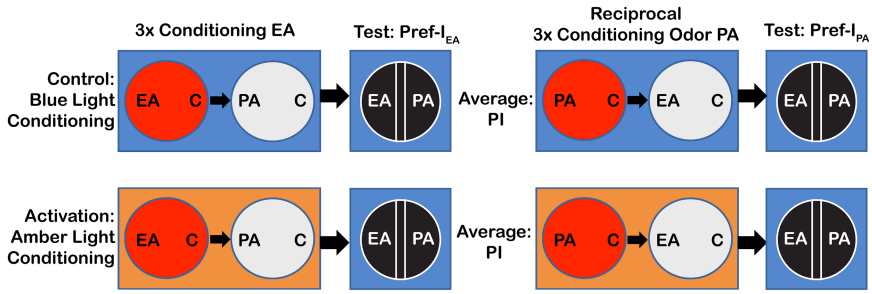

Figure 8. Behavioral discrimination assay and optogenetics. Larvae were conditioned for three cycles of an agarose fructose plate (red), carrying a container with one odor (here ethyl acetate [EA]) and a control container with mineral oil (C), followed by an agarose plate lacking fructose (light gray), but carrying a container with a different odor (here pentyl acetate [PA]) and a control container with mineral oil. Larvae were then tested by being placed on an oblong area in the middle of an agarose plate, with a choice of EA or PA, and a black background to provide contrast for counting larvae, and a conditioned preference index for EA (Pref-I_{EA}) was measured. A different group of larvae were conditioned and tested with reciprocal odor pairing. Learning was measured as a performance index (PI) averaged from Pref-I_{EA} and Pref-I_{PA}. (*Top* row) Control experiments were carried out in dim blue light. Optogenetic activation of CsChrimson was accomplished by amber light during the conditioning phases.

receptors (Bentley et al. 2016), and this may be the case for Oamb in PN terminals. sVUM1 neurons have dense core vesicles (DCV), and these might release peptides together with OA (Tao et al. 2019). However, it is known that OA is packed into vesicles by DVMAT-A (Greer et al. 2005) in *Drosophila*, and although we can not exclude the possibility of volume transmission rather than classical synapses as an extra mechanism of release, this has not been documented for OA.

Oamb is a GPCR that signals apparently through Gq, to release Ca^{2+} from intracellular stores (Balfanz et al. 2005; Morita et al. 2006); it may also elevate cAMP (Han et al. 1998), although this effect appears smaller (Balfanz et al. 2005). In adult *Drosophila*, Tomchik and Davis (2009) found that bath application of OA increased cAMP responses in PN axons. These results suggest that OA can excite PN neuron terminals via cAMP, and thus facilitate synaptic transmission. In agreement with this, presynaptic facilitation was observed in *Aplysia* sensory neurons through the cAMP/PKa pathway after exogenous expression of the OA receptor, Ap oa_1 (Chang et al. 2000).

Since we also observe GRASP signals between sVUM1 neurons and a minority of KCs, a cAMP-mediated mechanism in KCs could also facilitate synaptic transmission; elevating cAMP facilitates Ca^{2+} responses of MB neurons to stimulation by ACh (Tomchik and Davis 2009). The cAMP/PKA pathway in MB neurons can also affect the duration of excitation through a K^+-channel-mediated mechanism (Aoki et al. 2008). However, we did not observe Oamb receptor expression in KC dendrites.

An alternate mechanism of OA in plasticity is that subthreshold sensory input could be gated by OA to facilitate the detection of subthreshold signals. In the mammalian olfactory bulb, LC input facilitates the detection of peri-threshold stimuli and near-threshold rewarded odors (Jiang et al. 1996; Escanilla et al. 2012), via an increase in mitral cell excitability mediated by NA action on α1-adrenergic receptors (Ciombor et al. 1999; Hayar et al. 2001). Therefore, Oamb receptors in PN terminals in the calyx could potentially participate in plastic changes to facilitate the detection of behaviorally relevant sensory input in a given behavioral context.

Odor discrimination learning

We selected odorants as a dissimilar pair, EA and PA, that activate different sets of glomeruli in the AL (Kreher et al. 2008). On the other hand, odor mixtures, which we used as the basis of our similar odor pairs, often activate patterns in the olfactory centres that are a combination of single odorant response in honeybees (Joerges et al. 1997) and mice (Grossman et al. 2008). How this pattern of activity is translated into perceptual similarity is not entirely clear, but representations in the cortex do correlate with behavioral discrimination (Chapuis and Wilson 2012). Reinforced olfactory discrimination has been used in honeybees (Stopfer et al. 1997), *Drosophila* (Lin et al. 2014), and mammals (Linster and Cleland 2001), to test neural mechanisms of odor discrimination.

Here we observed that optogenetic activation of five OA neurons, including the VUM1 neurons, compromised discrimination of similar odors in an appetitive conditioning paradigm, either during conditioning, or during testing (Fig. 9). The anatomical organization of KCs in the calyx predicts that KCs are coincident detectors of multiple inputs; a single KC innervates about six calyx glomeruli, and therefore would fire selectively only when coincident inputs to a given KC are activated (Masuda-Nakagawa et al. 2005). This hypothesis is consistent with physiological recordings showing that KCs fire transiently with high selectivity in locust (Perez-Orive et al. 2002), and in *Drosophila* (Turner et al. 2008). This suggests a model in which KC responses would determine the selectivity to input and hence the discrimination ability of the calyx, that is, higher calyx input activity would result in low discrimination, with overlapping in odor representations by KCs, while lower input activity might improve discrimination at the expense of sensitivity. On the other hand too low input activity would make the system unable to discriminate. Our result is consistent with OA innervation affecting the selectivity of odor representations by KCs, both during formation of odor memory, and during recall. Based on the presence of OA receptors in PN terminals (Fig. 6), we hypothesize that VUM1 activation might modulate the gain of stimulus-driven PNs, increasing the magnitude and number of KCs responding, and thus making representations of similar odors by KCs overlap more, and lowering their discriminability. On the other hand, the representations of dissimilar odors might be distinct enough to be discriminable by the calyx circuit.

A role for OA as a reinforcer in appetitive associative learning has been shown in honeybees and flies. The honeybee VUMmx1 neuron has properties of a reinforcer; its depolarization could replace sugar reinforcement in appetitive learning (Hammer 1993), and injection of OA into the MB calyx induced memory consolidation (Hammer and Menzel 1998). On the other hand, it has been proposed that VUMmx1 learns about the value of the odor, and acts as a prediction error signal in appetitive learning (Menzel 2012). However, associative plasticity in the MBs in *Drosophila* is thought to reside mainly in the lobes rather than the calyx, for both appetitive (Schwaerzel et al. 2003; Schroll et al. 2006; Liu et al. 2012) and aversive learning (Aso et al. 2012, 2014). OA as a reinforcer in appetitive learning appears to act via Oamb expressed in PAM dopamine neurons that target the medial MB lobes. The *NP7088-GAL4* line that includes the fly equivalent of the honeybee VUMmx1, OA-VUMa2, did not induce and is not required for appetitive learning in adult *Drosophila* (Burke et al. 2012). In larvae, pPAM neurons that innervate the medial lobe appear to be involved in reward learning (Rohwedder et al. 2016). We found Oamb::GFP at the tip and around the MB medial lobe (Fig. 7), suggesting this as a potential site of integration of appetitive

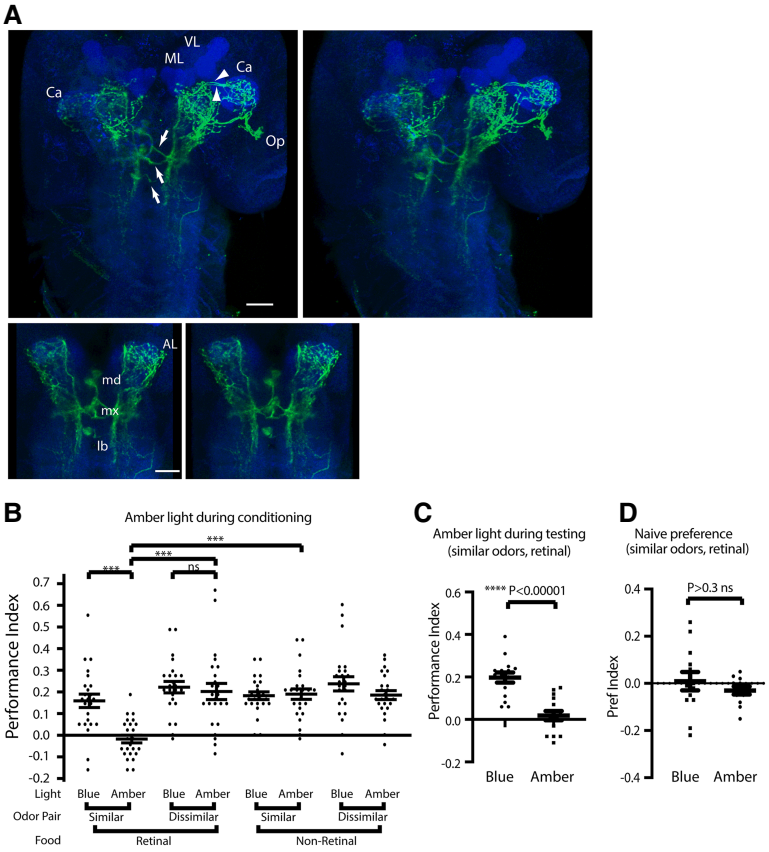

Figure 9. Activation of a small subset of OA neurons including the sVUM1 neurons disrupts odor discrimination but not learning. (*A*) Third-instar larvae of genotype *w, FRT.GAL80*; *Tdc2-LexA(II)/LexAop2-FLPL(II)*; *GMR34A11-GAL4(III)/UAS-CsChrimson.mVenus(III)*, used for behavior, generated as in Figure 4A. The *top* panels show a pair of stereo images with CsChrimson.mVenus expressed in a subset of five sVUM neurons, including calyx-innervating sVUM1 neurons. Arrows indicate the secondary processes of the three sVUM1 clusters at the midline. The two tracts entering the calyx are indicated by arrowheads. Scale bar, 40 µm. The *bottom* row shows a close-up pair of stereo images of the vicinity of the SEZ; two cell bodies of sVUM1md cluster, two cell bodies of sVUM1mx cluster, and one cell body of the labial cluster are labeled. Antennal lobe (AL), calyx (Ca), optic lobe (Op), MB medial (ML), and vertical (VL) lobes act as landmarks. Scale bar, 20 µm. (*B*) Activation of the neurons labeled in *A* by CsChrimson in the presence of retinal and amber light (applied during conditioning), abolishes odor choice learning using a similar odor pair, compared with controls exposed to blue light, lacking retinal, or tested with a dissimilar odor pair. No effect of CsChrimson activation is seen on learning using a dissimilar odor pair. Planned statistical comparisons shown are *t*-tests. (***) $P<0.0001$, (NS) $P>0.6$. $n=24$. An ANOVA test of all data from two experimenters showed no significant effect of experimenter alone, or as interactions with other factors ($P>0.2$). ANOVA tests showed no significant effect of odor alone ($P>0.03$, not significant with multiple testing), retinal alone ($P>0.4$), or light alone ($P>0.2$), when comparisons that would have included the retinal, amber, similar combination with the strong effect were excluded. (*C*) Amber light abolishes learning using a similar odor pair in the presence of retinal, if applied only during testing, after conditioning in blue light ($P<10^{-5}$, *t*-test, $n=15$). A two-way ANOVA showed no significant difference between two experimenters ($P>0.25$), nor any interaction between experimenter and light ($P>0.7$). (*D*) No effect of light color on naive odor preference. Larvae of the same genotype, grown on retinal-containing food as in *B* and *C*, were tested for naive odor preferences under either blue or amber light. No effect was detected (paired *t*-test, $n=12$).

reinforcement for learning. Furthermore, Oamb is required in KCs for adult appetitive learning (Kim et al. 2013), suggesting some direct input of an OA-encoded appetitive signal into KCs; the localization of Oamb to MB lobes (Crittenden et al. 1998) is consistent with OA signaling on KC axons in the lobes rather than dendrites in the calyx. Taken together, OA action as mediating reward in associative learning might occur via unidentified inputs into dopaminergic neurons or KC lobes.

sVUM1 neurons innervate the AL, and synapse with inhibitory interneurons (Supplemental File S1); therefore, OA can modulate the processing of olfactory signals. In honeybee, injection of OA in the antennal lobes impairs memory acquisition and recall but not odor discrimination (Farooqui et al. 2003). Noradrenalin in mammals has a role in olfactory memory formation by affecting the inhibitory network in the olfactory bulb (for review, see Kaba and Nakanishi 1995). Therefore, OA is likely to be involved in synaptic plasticity in the first relay of the olfactory pathway, sharpening its output. In our studies we tested odor discrimination ability, and our results favor the interpretation that OA acts by changing the efficacy of synaptic input to the MBs, at the calyx. A role in gating behaviorally relevant sensory input is favored by our behavioral data, and is also suggested as a role of OA in modulating the threshold response of peripheral sensory receptors and afferents in insects and NA in the CNS of mammals (Berridge and Waterhouse 2003). Our behavioral data could be interpreted to result from an increase in the levels of sensitivity, at expense of discrimination, to meet the demands of changes in behavior, signaled by OA.

Perspectives

Sensory representations are dynamically modified by higher brain signaling, according to behavioral states such as attention, expectation, and behavioral task; and LC (locus coeruleus) activation in mammals and OA activation in insects correlate with changes in behavioral states. Mammalian olfactory neuropiles are densely innervated by noradrenergic input, similar to the dense innervation of the AL and calyx by OA sVUM1 neurons in insects. The innervation of sVUM1 neurons throughout the calyx, and their potential synaptic connections to PNs, KCs, APL, and Odd neurons, mean that OA could induce a network level switch either by gating input afferent activity, and/or by interacting with the KC/APL feedback loop, and thus also affecting the output activity from the calyx—not only through KCs but also potentially via the Odd neurons. Behavioral demands would determine the balance between sensitivity and discrimination via OA; whether to escape from a predator at all cost, or the need for fine discrimination to recognize food.

Materials and Methods

Genetics and molecular biology

Fly stocks

Flies were raised on standard cornmeal medium at 25°C and subjected to a 12-h day/night cycle. Stocks used are listed in Table 1.

Table 1. *Drosophila* stocks used

Genotype	Source	Reference	RRID	Use	Figure
NP2631-GAL4 (II)	T. Awasaki, K. Ito	Masuda-Nakagawa et al. 2014	DGGR_104266	APL neuron	3A,E, 4D
NP0732-GAL4 (I)	T. Awasaki, K. Ito	Masuda-Nakagawa et al. 2014	DGGR_112307	APL neuron	6B
NP225-GAL4 (II)	T. Awasaki, K. Ito	Masuda-Nakagawa et al. 2005	DGGR_112095	PN	3A,B, 6A,D 7A
OK263-GAL4 (II)	C.J.O., L.M.M.-N.	This work		Odd neurons	3A,D, 4C, 6C
Mef2-GAL4 (III) (also known as *MB247-GAL4)*	BDSC 50742	Zars et al. 2000		KCs	3A,C
GMR34A11-GAL4 (III)	BDSC 49767	Jenett et al. 2012	BDSC_49767	sVUM1 neuron	4A, 9
Tdc2-GAL4 (II)	BDSC 9313	Cole et al. 2005	BDSC_9313	OA neuron	1, 2, 3F, 7D
Tdc2-LexA (II)	S. Certel, S. Waddell	Burke et al. 2012		OA neuron	3A,C, 4
Tdc2-LexA (III)	S. Certel, S. Waddell	Burke et al. 2012		OA neuron	3A,B,D,E
GMR34A11-LexA (II)	BDSC 52755	Jenett et al. 2012	BDSC_52755	sVUM1	4A, 9
NP225-GAL4 (II); Tdc2-LexA(III)		This work		GRASP	3A,B
OK263-GAL4; Tdc2-LexA(III)		This work		GRASP	3A,D, 4C
NP2631-GAL4; Tdc2-LexA(III)		This work		GRASP	3A,E, 4D
Tdc2-LexA (II); Mef2-GAL4		This work		GRASP	3A,C
Tdc2-LexA (II); GMR34A11-GAL4 (III)		This work		sVUM1 intersection	4A, 9
UAS-mCD8::GFP (III)	BDSC 5130	Lee and Luo 1999	BDSC_5130	mCD8::GFP reporter	2D, 3F, 6B,C, 7D
10XUAS-IVS-mCD8::RFP (attP40) (II)	BDSC 32219	Pfeiffer et al. 2010	BDSC_32219	mCD8::RFP reporter	6, 7A
13XLexAOp-mCD8::GFP (III)	BDSC 32203	Pfeiffer et al. 2010	BDSC_32203	mCD8::GFP reporter, to verify *LexA* stocks	
UAS-CD4::tdTomato (II)	BDSC 35841	Han et al. 2011	BDSC_35841	Neuronal polarity	2A
UAS-nSyb::GFP (III)	M. Ramaswami	Estes et al. 2000		Neuronal polarity	2A
UAS-CD4::tdTomato (II); UAS-nSyb::GFP (III)		This work		Neuronal polarity	2A
UAS-Syt::GFP UAS-DenMark::mCherry (III)	BDSC 33065	Nicolaï et al. 2010	BDSC_33065	Neuronal polarity	2B,C
10XUAS-IVS-mCD8::RFP, 13XlexAOp2-mCD8::GFP (X)	BDSC 32229	Pfeiffer et al. 2010	BDSC_32229	Double reporter, to verify *GAL4 LexA* stocks	
UAS-CD4::spGFP1-10	K. Scott	Gordon and Scott 2009		GRASP	3
LexAop-CD4::spGFP11	K. Scott	Gordon and Scott 2009		GRASP	3
LexAOp2-IVS > stop > spGFP11::CD4::HA-T2A-Brp::mCherry (attP2), UAS-spGFP1-10::CD4, UAS- HRP::CD2	C.-H. Lee	Karuppudurai et al. 2014		Single-cell GRASP	4B–D
P{hsFLP}12 y w; +; LexAOp2-IVS > stop > spGFP11::CD4::HA-T2A-Brp::mCherry (attP2), UAS-spGFP1-10::CD4, UAS- HRP::CD2		This work		Single-cell GRASP	4B–D
P{hsFLP}12 y w; CyO/Sco	Fly Facility, Department of Genetics		BDSC_1929	Single-cell GRASP	4B–D
pBPhsFlp2::PEST(attP3); +; HA_V5_FLAG_OLLAS (III)	M. Landgraf	Nern et al. 2015	BDSC_64086	Multicolor FlpOut (MCFO-2)	1
Tub84B(FRT-GAL80)1, w; Bl/CyO; TM2/TM6B	BDSC 38879		BDSC_38879	sVUM1 intersection	4A, 9
P{8xLexAop2-FLPL}attP40 (II)	B. Pfeiffer, Janelia		BDSC_55820	sVUM1 intersection	4A, 9
UAS-Chrimson.mVenus (III)	BDSC 55136	Klapoetke et al. 2014	BDSC_55136	Effector/reporter for intersectional lines	4A, 9
Tub84B(FRT-GAL80)1, w; P{8xLexAop2-FLPL} attP40(II); UAS-Chrimson.mVenus (III)		This work		sVUM1 intersection	4A, 9
y^1 *w*; +; Mi{MIC}Oamb*^{MI12417}	BDSC 57940	Venken et al. 2011	BDSC_57940	Progenitor of *Oamb::EGFP*	
y^1 *w*; +; Mi{PT-GFSTF.1}Oamb*$^{MI12417\text{-}GFSTF.1}$*/ TM6C*	Fly Facility, Department of Genetics	This work		Oamb::EGFP	6, 7A,B,C
UAS-mCD8::RFP; Oamb::EGFP		This work		Oamb::EGFP colocalization	6, 7A
Mi{MIC}Octβ1R^{MI05807}	BDSC 42119	Venken et al. 2011	BDSC_42119	Progenitor of *Octβ1R::EGFP*	
Mi{MIC}Octβ2R^{MI13416}	BDSC 59133	Venken et al. 2011	BDSC_59133	Progenitor of *Octβ2R::EGFP*	
Mi{MIC}Octβ2R^{MI06217}	BDSC 43050	Venken et al. 2011	BDSC_59133	Progenitor of *Octβ3R::EGFP*	
Mi{PT-GFSTF.2}Octβ1R$^{MI05807\text{-}GFSTF.2}$	BDSC 60236	Venken et al. 2011	BDSC_60236	Octβ1R::EGFP	
Mi{PT-GFSTF.2}Octβ2R$^{MI13416\text{-}GFSTF.2}$	Fly Facility, Department of Genetics	This work		Octβ2R::EGFP	

Continued

Table 1. *Continued*

Genotype	Source	Reference	RRID	Use	Figure
Mi{PT-GFSTF.0}Octβ3R$^{MI06217\text{-}GFSTF.0}$	Fly Facility, Department of Genetics	This work		Octβ3R::EGFP line, GFP intron phase 0	
Mi{PT-GFSTF.1}Octβ3R$^{MI06217\text{-}GFSTF.1}$	BDSC 60245	Nagarkar-Jaiswal et al. 2015	BDSC_60245	Octβ3R::EGFP line, GFP intron phase 1	

Includes all genotypes used for this study, including those that do not appear in figures.

Multicolor FlpOut

Multicolor FlpOut was performed according to Nern et al. (2015). Females of genotype *pBPhsFlp2::PEST(attP3); +; HA_V5_FLAG_OLLAS* ("MCFO-2") were crossed with male *Tdc2-Gal4* flies. Parents were left in vials to lay eggs for 24-h intervals. After another 24 h, larval progeny were heat shocked at 35°C–37°C by immersion in a heated circulated waterbath for 15–30 min, thus ensuring larvae were aged 24–48 h after egg laying (AEL) at the time of heat shock.

GRASP

Standard GRASP was according to Gordon and Scott (2009). A line carrying GRASP constructs *UAS-CD4::spGFP1-10* and *LexAop-CD4::spGFP11*, was crossed to individual *LexA GAL4* lines as needed: *NP225-GAL4(II); Tdc2-LexA(III)*, *OK263-GAL4(II); Tdc2-LexA(III)*, *NP2631-GAL4(II); Tdc2-LexA(III)*, or *Tdc2-LexA(II); Mef2-GAL4(III)* (Fig. 3), or to individual *GAL4* or *LexA* lines as controls (Supplemental Fig. S1). Reconstituted GFP was detected using rat monoclonal anti-GFP. This did not detect either of the GRASP components GFP1-10 or GFP11, when *Gal4* or *LexA* drivers were used alone (Supplemental Fig. S1). GRASP signals had to meet a criterion of occurring in two consecutive 0.5-µm confocal sections. For single-cell GRASP (Karuppudurai et al. 2014), we generated larvae carrying *P{hsFLP}*12, appropriate *GAL4* and *LexA* combinations, and a recombinant chromosome with insertions *LexAOp2-IVS>stop>spGFP11::CD4::HA-T2A-Brp::mCherry (attP2)*, *UAS-spGFP1-10::CD4,* and *UAS- HRP::CD2,* by generating a stock carrying *P{hsFLP}12 y w; +; LexAOp2-IVS>stop>spGFP11::CD4::HA-T2A-Brp::mCherry (attP2), UAS-spGFP1-10::CD4, UAS-HRP::CD2*, and crossing females of this stock to relevant *GAL4 LexA* males. To generate labeled single cells, parents were allowed to lay eggs initially for 24-h intervals, then for 6-h intervals in vials containing half the amount of food. At 0–24 h, 24–48 h, or later at 12–18 h, 18–24 h, or 24–30 h AEL, progeny were heat shocked as above for 10–50 min at 37°C. Progeny were incubated from RT until dissection of nontubby wandering third-instar larvae.

Generation of an EGFP–tagged Oamb line

The *Mi{MIC}Oamb^{MI12417}* insertion in coding intron 3 of *Oamb* at 3R:20697059, (BDSC stock 57940; henceforth referred to as *MI12417*) was verified by PCR using primers *MI12417-5F/MiMIC-5R1* for the 5′ end and *MI12417-3R/MiMIC-3F1* for the 3′ end (Table 2; Supplemental Fig. S2). Sequencing of these PCR products and alignment with the *Drosophila* genome sequence using BLASTN (Altschul et al. 1990; https://blast.ncbi.nlm.nih.gov) showed insertion of *MiMIC* at the recorded site of 3R 20697058-9 (Supplemental Figs. S3, S4). The location of the *MI12417* insertion site relative to *Oamb* coding exons was determined by using Oamb-B sequences for BLASTN and TBLASTN queries of the *Drosophila* genome assembly (Supplemental Fig. S5; http://flybase.org/blast). TMHMM (Sonnhammer et al. 1998; http://www.cbs.dtu.dk/services/TMHMM) was used to predict the amino acid coordinates of Oamb transmembrane (TM) domains (Supplemental Figs. 6, 7).

To insert an EGFP-encoding exon into the *MI12417* insertion by RMCE, we chose the splice phase-1 version of the *EGFP-FlAsH-StrepII-TEV-3xFlag* plasmid (DGRC 1306) (Venken et al. 2011) as recommended by the Baylor Gene Disruption Project (http://flypush.imgen.bcm.tmc.edu/pscreen/rmce/rmce.php?entry=RM00888). This was coinjected with a helper phiC31-integrase plasmid (Venken et al. 2011) by the *Drosophila* microinjection facility (Department of Genetics, University of Cambridge). Injected embryos were left to hatch into adult flies and crossed to a *y w* double balancer stock. RMCE events were identified by loss of the *MiMIC yellow*$^{+}$ marker in F1 progeny. Four PCR

Table 2. Primers

Primer	Sequence	Purpose
MiMIC-5R	CTTGAGATTAAGGTAGCTTACGC	Verifying Mi{MIC} insertion
MiMIC-3F	TGCAGGTCGACGAATTCAAC	Verifying Mi{MIC} insertion
MI12417-5F	CCACAATCAACGTCCTGCTC	Verifying Mi{MIC} insertion
MI12417-3R	GATTATCGCCACCACAGAGTC	Verifying Mi{MIC} insertion
MI05807-5F	TCCTTTCATTCCCGAGCACC	Verifying Mi{MIC} insertion
MI05807-3R	CTCGTTAACAATCGCTCGCC	Verifying Mi{MIC} insertion
MI13416-5F1	CGGAGTCACTGAGTAATGGCG	Verifying Mi{MIC} insertion
MI13416-5F2	ATGGCGAGTGGTATGAGCAG	Verifying Mi{MIC} insertion
MI13416-5F3	GTGCTCTAGATGGCGAGTGG	Verifying Mi{MIC} insertion
MI13416-5F4	ACCGAGGCTCATTAACACAG	Verifying Mi{MIC} insertion
MI13416-5F5	GAGGCTCATTAACACAGCGC	Verifying Mi{MIC} insertion
MI13416-3R	GCTGCCTCATTGAACTCCAG	Verifying Mi{MIC} insertion
MI06217-5F	GCAGGAGAACAGCGACAGTC	Verifying Mi{MIC} insertion
MI06217-3R	CCTGTCTCTGGAAGTAGGTCG	Verifying Mi{MIC} insertion
Orientation-MiL-F (OriF)	GCGTAAGCTACCTTAATCTCAAGAAGAG	Verifying GFP swap orientation
Orientation-MiL-R (OriR)	CGCGGCGTAATGTGATTTACTATCATAC	Verifying GFP swap orientation
EGFPdo-Seq-F (EGFP-F)	GGATGACGGCACCTACAAGAC	Verifying GFP swap orientation
EGFPdo-Seq-R (EGFP-R)	GTGGCTGTTGAAGTTGTACTC	Verifying GFP swap orientation

reactions were carried out to determine the orientation of the EGFP cassette in each recombinant *Oamb::EGFP* stock (Table 2) as described in Venken et al. (2011).

*Octβ*R EGFP *fusions*

For *Octβ1R* and *Octβ3R*, we used lines $Octβ1R^{MI05807\text{-}GFSTF.2}$ and $Octβ3R^{MI06217\text{-}GFSTF.1}$ (Bloomington stocks 60236 and 60245), respectively, as *Octβ1R::EGFP* and *Octβ3::EGFP* exon traps. For *Octβ2R*, we used $Mi\{MIC\}Octβ2R^{MI13416}$ to generate $Octβ2R^{MI13416\text{-}GFSTF.2}$ using a similar approach as that described above for *Oamb::EGFP*. We also generated a second *Octβ3::EGFP* exon trap, $Octβ3R^{MI06217\text{-}GFSTF.0}$, in a different reading frame from Bloomington stock 60245, to allow for the possibility of the *EGFP* exon being spliced as in transcripts *RJ* or *RK* (frame 0, with only *RJ* able to encode all seven TM domains), rather than *RF* or *RG* (frame 1). Positions of each insertion were confirmed by PCR and sequencing similarly to *Oamb*, using primers as described in Table 2.

Molecular methods

Genomic DNA was extracted from 15–30 flies (1–7 d after eclosion) and homogenized in 100 mM Tris-HCl (pH 8.5), 80 mM NaCl (Sigma 31434), 5% sucrose (Sigma S0389), 0.5% SDS (Sigma L4509), and 50 mM Na-EDTA (Sigma ED2SS) (pH 8.0). The homogenate was incubated with RNase A (Roche 10109142001) for 1 h at 37°C followed by Proteinase K (Roche 03115887001) for 1 h at 50°C, and purified with phenol–chloroform (Sigma 77617) and chloroform (Sigma C2432). DNA was precipitated with 0.6 vol of isopropanol (Sigma 59304) and washed with 75% ethanol (Sigma E7023), dried overnight at room temperature and resuspended in 10 mM Tris-HCl (pH 8.0) (Sigma T6066).

PCR reactions (20 µL) contained 0.4 µL or 1 µL of genomic DNA, 1 µL of each 10 µM primer (Sigma), 2 µL of 10× PCR buffer (Qiagen 203203), 0.4 µL of 10 µM dNTP mix (Roche 11581295001), 0.08 µL of 5 U/µL HotStarTaq DNA polymerase (Qiagen 203203), and 15.1 µL or 14.5 µL milliQ water. PCR cycling in a G-Storm Thermal Cycler (GS4) was 15 min at 95°C; 40 cycles of denaturation for 30 sec at 94°C, annealing for 30 sec at 60°C, and elongation for 1 min at 72°C; and a final elongation step for 10 min at 72°C. PCR products were loaded with 6× DNA gel-loading dye (Thermo Fisher R0611) on a 1% agarose gel (LifeTech 16500500; 1× TBE buffer, LifeTech 16500500) with GelRed (Biotium 41003-T) for gel electrophoresis. A 100-bp DNA ladder was used as a marker (LifeTech 15628019). PCR products were purified using the Qiaquick PCR purification iit (Qiagen, 28104), and sequenced at the Department of Biochemistry Sequencing Facility (University of Cambridge).

Immunohistochemistry and confocal imaging

Third-instar wandering larval brains (144–176 h AEL) were dissected in cold PBS (Sigma P4417), fixed in 4% formaldehyde (Polysciences 18814)/PEM buffer (0.1 M PIPES [Sigma P1851], 2 mM EGTA [Sigma E3889], 1 mM $MgSO_4$, NaOH) for 2 h at 4°C, washed three times for 10 min (or four times for 15 min) in 0.3% Triton-X (Sigma T8787) in PBS (PBT), and incubated in 10% NGS (normal goat serum; Vector Laboratories S-1000) in 0.3% PBT for 1 h at room temperature. Brains were incubated in primary antibody in 10% NGS-0.3% PBT for 2–3 d at 4°C on a minidisk rotor (Biocraft BC-710), washed three times for 15 min with 0.3% PBT, and further incubated in secondary antibody in 10% NGS for 2–3 d at 4°C again on the minidisk rotor. Brains were finally washed once for 15 min with PBT, followed by three times for 10 min with PBS, and left in 50% glycerol/PBS for at least one night at 4° C prior to imaging.

Primary and secondary antibodies are listed in Table 3. Brains were incubated in primary antibody for two to three nights at 4°C, washed three times in PBT for 15-min, and incubated in secondary antibody for two to three more nights. To reduce background with the polyclonal chicken anti-GFP (Abcam Ab13970), it was preincubated with *MI12417* larval brains, which do not express GFP. Fifty *MI12417* larval brains were incubated in 1:20 chicken anti-GFP in 10% NGS in 0.3% PBT overnight at 4°C. A further 50 *MI12417* larval brains were added and further incubated over two nights at 4°C. Mounting and orientation of brains for image acquisition was as described in the Supplemental Material in Masuda-Nakagawa et al. (2009). Imaging was carried out using a Zeiss LSM710 Confocal Microscope with a 40× NA1.3 oil objective. Images were processed using ImageJ software (https://imagej.nih.gov/ij/download.html).

Behavioral assay

Larval culture

Males of genotype *w; Tdc2-LexA; GMR34A11-GAL4/TM6B* were crossed to females of genotype *Tub84B(FRT-GAL80)1, w; LexAop-FLP; UAS-Chrimson.mVenus/TM6B* to generate F1 larvae in which *UAS-Chrimson.mVenus* could be expressed only in cells expressing both *Tdc2-LexA* and *GMR34A11-GAL4*, in which LexA-dependent *FLP* expression had removed the GAL4 inhibitor GAL80. Larvae were allowed to develop in food vials containing 200 µM all-*trans*-retinal (Sigma R2500), in the dark at 21°. For both the retinal and nonretinal food vials, transfer of adults into new vials was performed both in the morning and in the evening, to then collect them after 108–120 h in the case of nonretinal vials at 25°C, and after 132–144 h for those kept in retinal vials at 23°C. Reagents for this and other behavioral work are listed in Table 4.

Behavioral arena

Petri dishes (8.5-cm) containing agarose were prepared the day before use, using 100 mL of distilled water with 0.9% agarose (Sigma A9539). Fructose Petri dishes were prepared similarly, but containing 35% fructose (Sigma 47740). Petri dishes had perforated lids to facilitate creation of odorant gradients within the dish, generated by sucking air away using a benchtop fume extractor (Sentry Air Systems SS-200-WSL) at the back of the assay platform. Odorants were diluted in paraffin oil (Sigma-Aldrich 76235), and 10-µL aliquots were pipetted with a cotton filled tip, immediately before conditioning or test, into custom-built Teflon containers with pierced lids (seven holes), made in the Physiology Department workshop in the University of Cambridge, based on samples kindly provided by B. Gerber.

Light apparatus

Our optogenetics apparatus was constructed as described by de Vries and Clandinin (2013) for activation of ChR. We modified it to shine amber light to activate CsChrimson. A BK Precision 1698 model DC power pack was connected to a pulse generator, driving four sets of amber light LEDs (591 nm), Luxeon star Amber LED on Tri-Star Base, 330 lm at 350 mA (SP-03-A5). The irradiance on the platform was 0.06 $\mu W/mm^2$ on average (24 µW on a 20 × 20-mm sensor) on the 8.5-cm plate. The pulse generator was custom-built by the Psychology Department workshop of the University of Cambridge, to deliver 10-msec pulses at 10 Hz for 30 sec, followed by 30 sec without pulses. This cycle was repeated five times, making a conditioning step of 5 min in total. The power supply was run at 17-mV constant voltage. This pulse frequency and width were chosen to replicate the activity of the only recorded sVUM1 neuron, the honeybee sVUMmx1, when activated by a sucrose reward (Hammer 1993). Reagents are listed in Table 4.

Behavior conditioning

Third-instar larvae were collected from vials using a stainless steel SANPO 355 µm/m and washed with tap water. Larvae were washed twice by transferring through a drop of tap water, and then placed on the conditioning agarose plate (35% fructose) with the help of a paint brush.

One conditioning cycle consisted of placing larvae in a fructose dish exposed to the odor to be conditioned with for 5 min, and then washing in two drops of water to clean them of fructose, before transferring to an agarose dish, where larvae were exposed to

Table 3. Antibodies

	Host	Source	RRID	Dilution	Experiment or figures
Antibody					
Anti-GFP	Rat, monoclonal	Nacalai 440426 (clone GF090R)	AB_2314545	1:1000	GRASP (3B–E) UAS-CD8::GFP
Anti-GFP	Chicken, polyclonal	Abcam Ab13970	AB_300798	1:1000/1:2000	Oamb::EGFP (6,7)
Anti-GFP	Rabbit, polyclonal	Invitrogen A11122	AB_221569	1:1000/1:2000	
Anti-GFP	Rabbit, polyclonal	Abcam Ab290	AB_303395	1:800	
Anti-DsRed	Rabbit, polyclonal	Clontech 632496	AB_10013483	1:1000	UAS-tdTom (2A), UAS-DenMark (2B,C), Brp::mCherry (4B–D) UAS-RFP (6, 7)
Anti-GABA	Rabbit, polyclonal	Sigma A2052	AB_477652	1:1000	3E,F, 6B
Anti-OA	Rabbit, polyclonal	MoBiTec 1003GE	AB_2314999	1:1000	3B–E
Anti-Dlg	Mouse, monoclonal	DSHB 4F3	AB_528203	1:200	2–4, 6, 7, 9
Anti-FLAG	Mouse, monoclonal	Sigma F1804	AB_262044	1:4000	MCFO
Anti-HA	Rat, monoclonal	Roche 3F10	AB_2314622)	1:1000	MCFO (1A,B)
Anti-V5	Chicken, polyclonal	Abcam Ab1993	AB_302743	1:1000	MCFO (1A,B)
Secondary antibody					
Anti-rat Alexa 488	Goat, polyclonal	Invitrogen A11006	AB_2534074	1:200	
Anti-rat Alexa 594	Goat, polyclonal	Invitrogen A11007	AB_10561522	1:200	
Anti-chicken Alexa 488	Goat, polyclonal	Invitrogen A11039	AB_142924	1:200	
Anti-rabbit Alexa 488	Goat, polyclonal	Invitrogen A11034	AB_2576217	1:200	
Anti-rabbit Alexa 568	Goat, polyclonal	Invitrogen A11036	AB_10563566	1:200	
Anti-mouse Alexa 647	Goat, polyclonal	Invitrogen A21236	AB_141725	1:200	
Anti-rabbit Alexa 647	Goat, polyclonal	Invitrogen A21245	AB_2535813	1:200	
Anti-chicken Alexa 568	Goat, polyclonal	Invitrogen A11041	AB_2534098	1:200	

the other odor of the pair for 5 min without the reinforcer. This cycle was repeated three times. For experiments involving activation of OA neurons, the three conditioning cycles with reinforcer present and the three nonreinforced cycles were carried out under pulses of amber light (Fig. 9). For controls without activation of CsChrimson, conditioning was performed as with amber light but under dim blue light, using an aquarium lamp, covered with paper to decrease its intensity.

Containers were placed at 1 cm from the side of the dish (Fig. 8). One container was filled with odor while the one on the opposite side contained mineral oil. One experimenter (ADM) placed containers consistently at the same position throughout conditioning cycles; the other (MM) alternated oil and odor containers between sides for each 5 min of the three cycles, to avoid any inadvertent effects of illumination.

Odor dilutions

Our choice of odor was based on the cluster analysis of Kreher et al. (2008). We measured the response index (RI) of Canton-S (CS) wild-type larvae to diverse odorants of the Kreher odor panel at different intensities, aiming to reach an RI of >0.5, according to the widely used protocol of Monte et al. (1989), Rodrigues and Siddiqi (1978), and Kreher et al. (2008). RI was defined as RI = (S − C)/(S + C), where S is the number of larvae on the odor side, and C is the number of larvae on the diluent side, after 5 min.

Table 4. Other reagents

Reagent	Source	Experiment or figures
Paraffin oil	Sigma-Aldrich 76235	Behavior
Pentyl acetate	Sigma-Aldrich 109584	Behavior
Ethyl acetate	Sigma-Aldrich 319902	Behavior
Ethanol	Sigma-Aldrich 32221	Behavior
All-*trans*-retinal (ATR)	Sigma-Aldrich R2500	Behavior
D-(-)-fructose	Sigma-Aldrich 47740	Behavior
Agarose	Sigma-Aldrich A9539	Behavior

We selected ethylacetate (EA; Sigma-Aldrich 319902) at 1:2000 dilution, which gave RI = 0.57 ± 0.04 (mean ± SEM, $n = 12$), in CS third-instar larvae. To establish a dissimilar odor pair, we selected pentyl acetate (PA; also known as amyl acetate or n-amyl acetate; Sigma-Aldrich 109584). EA and PA are homologous esters that differ by a length of three carbons. Since the RI for EA is higher than PA (Cobb and Dannet 1994), we used odor balancing to determine the dilution of PA that would balance EA, that is, a preference index (Pref-I) of around 0 given a choice between the two odors, first using CS wild-type larvae (Supplemental Methods in the Supplemental Material), and subsequently with larvae of the genotype used for learning and discrimination behavior, *w, FRT.GAL80; Tdc2-LexA/LexAop2-FLPL; GMR34A11-GAL4 / UAS-CsChrimson.mVenus,*. Pref-I was calculated as (number of larvae in EA) − (number of larvae in PA)/(total number of larvae) (Scherer et al. 2003). A negative Pref-I means preference toward PA. Dilutions of EA at 1:2000 and PA at 1:500 gave a Pref-I of close to 0, and these were used as dissimilar odors in conditioning experiments.

Testing

Larvae were tested by placing them on an agarose plate carrying a container with EA (1:2000) on one side, and a container with PA (1:500) on the opposite side (dissimilar odors), or a container with EA:PA 4:1 and one with EA:PA 1:4 (similar odors; mixes were made using the same dilutions as in the dissimilar odor pair). Testing was performed under dim blue light, as used during conditioning, for 5 min. Larvae were counted on the side of the conditioned odor, the unconditioned odor, and in the neutral zone in the middle. A single performance index (PI) (Selcho et al. 2009) was calculated as $PI = [N_{\text{conditioned (A+)}} - N_{\text{unconditionsed (B)}}]/N_{\text{total}}$, where $N_{\text{conditioned (A+)}}$ is the number of larvae on the side of the conditioned odor, $N_{\text{unconditioned (B)}}$ is the number of larvae on the side of the unconditioned odor, and N_{Total} is the number of larvae on the side of conditioned A+ odor, unconditioned odor B, and middle zone.

Since we performed a reciprocal conditioning run, to avoid nonassociative effects, a different sample of larvae were conditioned in parallel, with the previously unconditioned odor. An average performance index (PI) was calculated from the two groups of larvae (A+/B and A/B+) conditioned reciprocally, using the formula PI = (PI odor A+/B − PI odor A/B+)/2.

To test the effect of amber light during testing, the same procedure of differential conditioning with similar odors, and larvae grown in retinal-supplemented food, was performed by conditioning in blue light, and then applying either amber or blue light during testing.

Controls for the effect of light on similar odor responses

To test for any bias of larval behavior caused by amber light alone, larvae of the experimental genotype were exposed to light, in similar light conditions as in the conditioning trainings, but without fructose, and tested for their odor preferences. Thirty larvae grown in retinal food were exposed to the pair of similar odors on opposite sides of the dish, for 5 min, under either blue light or amber light, and their preference index calculated. Containers were swapped in order to exclude bias on illumination. Trials with dissimilar odors were also included.

Statistical analysis

Single planned comparisons were performed using *t*-tests in Microsoft Excel. A four-factor ANOVA using SPSS software was used to test whether performance index was affected by food type (retinal vs. nonretinal), light (blue vs. amber), odor pairs (similar pair vs. dissimilar pair), or experimenter (either of two). Effects of experimenter on learning scores were tested using two-way ANOVA tests in GraphPad Prism 8.0 and found to be nonsignificant ($P > 0.2$). Planned comparisons between the effects of retinal/nonretinal, amber/blue light, and similar/dissimilar odors were also confirmed in GraphPad Prism using Welch's *t*-test (not assuming equal SD) and by a nonparametric Mann–Whitney test. All distributions are expressed as mean ± standard error of the mean throughout.

Raw data and analyses files underpinning this article are available at https://doi.org/10.17863/CAM.60610.

Acknowledgments

We thank B. Gerber for odor containers; A. Cardona for access and training on CATMAID; T. Awasaki, S. Certel, K. Ito, M Landgraf, T. Lee, C.H.-Lee, B Pfeiffer, M. Ramaswami, K. Scott, J. Truman, and the Bloomington *Drosophila* Stock Center (BDSC) for numerous fly stocks; the Cambridge Genetics Department Fly Facility for stocks and microinjections; and the Developmental Studies Hybridoma Bank (DSHB), University of Iowa, for antibodies. We thank M. Morgan for help in building optogenetic illumination apparatus. J.Y.H.W. was supported by a Medical Research Council Studentship, and M.M. was supported by a UK Genetics Society "Genes & Development" summer scholarship and an award from the Bedford Fund, King's College Cambridge. T.B. was funded by a Biotechnology and Biological Sciences Research Council (BBSRC) Doctoral Training Program summer placement grant. This work was supported by BBSRC grants BB/I022651/1 and BB/N007948/1, and an Isaac Newton Trust award to L.M.M.-N. and C.J.O.

Author contributions: L.M.M.-N. and C.J.O. designed the experiments. J.Y.H.W., B.A.W., T.B., M.M., A.D.M., L.M.M.-N., and S.W.Z. performed the experiments. L.M.M.-N., B.A.W., J.Y.H.W., C.J.O., M.M., and A.D.M. analyzed the data. L.M.M.-N. drafted and wrote the manuscript.

References

Altschul SF, Gish W, Miller W, Myers EW, Lipman DJ. 1990. Basic local alignment search tool. *J Mol Biol* **215:** 403–410. doi:10.1016/S0022-2836(05)80360-2

Aoki K, Kosakai K, Yoshino M. 2008. Monoaminergic modulation of the Na^+-activated K^+ channel in kenyon cells isolated from the mushroom body of the cricket (*Gryllus bimaculatus*) brain. *J Neurophysiol* **100:** 1211–1222. doi:10.1152/jn.90459.2008

Aso Y, Herb A, Ogueta M, Siwanowicz I, Templier T, Friedrich AB, Ito K, Scholz H, Tanimoto H. 2012. Three dopamine pathways induce aversive odor memories with different stability. *PLoS Genet* **8:** e1002768. doi:10.1371/journal.pgen.1002768

Aso Y, Sitaraman D, Ichinose T, Kaun KR, Vogt K, Belliart-Guérin G, Plaçais PY, Robie AA, Yamagata N, Schnaitmann C, et al. 2014. Mushroom body output neurons encode valence and guide memory-based action selection in *Drosophila*. *Elife* **3:** e04580. doi:10.7554/eLife.04580

Aston-Jones G, Cohen JD. 2005. An integrative theory of locus coeruleus-norepinephrine function: adaptive gain and optimal performance. *Annu Rev Neurosci* **28:** 403–450. doi:10.1146/annurev.neuro.28.061604.135709

Balfanz S, Strünker T, Frings S, Baumann A. 2005. A family of octapamine receptors that specifically induce cyclic AMP production or Ca^{2+} release in *Drosophila melanogaster*. *J Neurochem* **93:** 440–451. doi:10.1111/j.1471-4159.2005.03034.x

Bauknecht P, Jékely G. 2017. Ancient coexistence of norepinephrine, tyramine, and octopamine signaling in bilaterians. *BMC Biol* **15:** 6. doi:10.1186/s12915-016-0341-7

Bentley B, Branicky R, Barnes CL, Chew YL, Yemini E, Bullmore ET, Vértes PE, Schafer WR. 2016. The multilayer connectome of *Caenorhabditis elegans*. *PLoS Comput Biol* **12:** e1005283. doi:10.1371/journal.pcbi.1005283

Berridge CW, Waterhouse BD. 2003. The locus coeruleus-noradrenergic system: modulation of behavioral state and state-dependent cognitive processes. *Brain Res Rev* **42:** 33–84. doi:10.1016/S0165-0173(03)00143-7

Bräunig P, Pflüger HJ. 2001. The unpaired median neurons of insects. *Adv In Insect Phys* **28:** 185–266. doi:10.1016/S0065-2806(01)28011-4

Brembs B, Christiansen F, Pflüger HJ, Duch C. 2007. Flight initiation and maintenance deficits in flies with genetically altered biogenic amine levels. *J Neurosci* **27:** 11122–11131. doi:10.1523/JNEUROSCI.2704-07.2007

Burke CJ, Huetteroth W, Owald D, Perisse E, Krashes MJ, Das G, Gohl D, Silies M, Certel S, Waddell S. 2012. Layered reward signalling through octopamine and dopamine in *Drosophila*. *Nature* **492:** 433–437. doi:10.1038/nature11614

Busch S, Selcho M, Ito K, Tanimoto H. 2009. A map of octopaminergic neurons in the *Drosophila* brain. *J Comp Neurol* **513:** 643–667. doi:10.1002/cne.21966

Cantarelli M, Marin B, Quintana A, Earnshaw M, Court R, Gleeson P, Dura-Bernal S, Silver RA, Idili G. 2018. Geppetto: a reusable modular open platform for exploring neuroscience data and models. *Philos Trans R Soc B Biol Sci* **373:** 20170380. doi:10.1098/rstb.2017.0380

Chang DJ, Li XC, Lee YS, Kim HK, Kim US, Cho NJ, Lo X, Weiss KR, Kandel ER, Kaang BK. 2000. Activation of a heterologously expressed octopamine receptor coupled only to adenylyl cyclase produces all the features of presynaptic facilitation in *Aplysia* sensory neurons. *Proc Natl Acad Sci* **97:** 1829–1834. doi:10.1073/pnas.97.4.1829

Chapuis J, Wilson DA. 2012. Bidirectional plasticity of cortical pattern recognition and behavioral sensory acuity. *Nat Neurosci* **15:** 155–161. doi:10.1038/nn.2966

Ciombor KJ, Ennis M, Shipley MT. 1999. Norepinephrine increases rat mitral cell excitatory responses to weak olfactory nerve input via α-1 receptors in vitro. *Neuroscience* **90:** 595–606. doi:10.1016/S0306-4522(98)00437-0

Cobb M, Dannet F. 1994. Multiple genetic control of acetate-induced olfactory responses in *Drosophila melanogaster* larvae. *Heredity* **73:** 444–455. doi:10.1038/hdy.1994.192

Cole SH, Carney GE, McClung CA, Willard SS, Taylor BJ, Hirsh J. 2005. Two functional but noncomplementing *Drosophila* tyrosine decarboxylase genes: distinct roles for neural tyramine and octopamine in female fertility. *J Biol Chem* **280:** 14948–14955. doi:10.1074/jbc.M414197200

Crittenden JR, Skoulakis EMC, Han KA, Kalderon D, Davis RL. 1998. Tripartite mushroom body architecture revealed by antigenic markers. *Learn Mem* **5:** 38–51.

Davison IG, Ehlers MD. 2011. Neural circuit mechanisms for pattern detection and feature combination in olfactory cortex. *Neuron* **70:** 82–94. doi:10.1016/j.neuron.2011.02.047

Deady LD, Sun J. 2015. A follicle rupture assay reveals an essential role for follicular adrenergic signaling in *Drosophila* ovulation. *PLoS Genet* **11:** 1–21. doi:10.1371/journal.pgen.1005604

de Vries SEJ, Clandinin T. 2013. Optogenetic stimulation of escape behavior in *Drosophila melanogaster*. *J Vis Exp* **2013:** 50192. doi:10.3791/50192

Eichler K, Li F, Litwin-Kumar A, Park Y, Andrade I, Schneider-Mizell CM, Saumweber T, Huser A, Eschbach C, Gerber B, et al. 2017. The complete connectome of a learning and memory centre in an insect brain. *Nature* **548:** 175–182. doi:10.1038/nature23455

Escanilla O, Alperin S, Youssef M, Ennis M, Linster C. 2012. Noradrenergic but not cholinergic modulation of olfactory bulb during processing of near threshold concentration stimuli. *Behav Neurosci* **126:** 720–728. doi:10.1037/a0030006

Estes PS, Ho GLY, Narayanan R, Ramaswami M. 2000. Synaptic localization and restricted diffusion of a *Drosophila* neuronal synaptobrevin: green fluorescent protein chimera in vivo. *J Neurogenet* **13:** 233–255. doi:10.3109/01677060009084496

Farooqui T, Robinson K, Vaessin H, Smith BH. 2003. Modulation of early olfactory processing by an octopaminergic reinforcement pathway in the honeybee. *J Neurosci* **23:** 5370–5380. doi:10.1523/JNEUROSCI.23-12-05370.2003

Gilbert CD, Li W. 2013. Top-down influences on visual processing. *Nat Rev Neurosci* **14:** 350–363. doi:10.1038/nrn3476

Gire DH, Restrepo D, Sejnowski TJ, Greer C, DeCarlos JA, Lopez-Mascaraque L. 2013. Temporal processing in the olfactory system: can we see a smell? *Neuron* **78:** 416–432. doi:10.1016/j.neuron.2013.04.033

Gordon MD, Scott K. 2009. Motor control in a *Drosophila* taste circuit. *Neuron* **61:** 373–384. doi:10.1016/j.neuron.2008.12.033

Gottfried JA. 2009. Function follows form: ecological constraints on odor codes and olfactory percepts. *Curr Opin Neurobiol* **19:** 422–429. doi:10.1016/j.conb.2009.07.012

Greer CL, Grygoruk A, Patton DE, Ley B, Romero-Calderon R, Chang HY, Houshyar R, Bainton RJ, DiAntonio A, Krantz DE. 2005. A splice variant of the *Drosophila* vesicular monoamine transporter contains a conserved trafficking domain and functions in the storage of dopamine, serotonin, and octopamine. *J Neurobiol* **64:** 239–258. doi:10.1002/neu.20146

Grossman KJ, Mallik AK, Ross J, Kay LM, Issa NP. 2008. Glomerular activation patterns and the perception of odor mixtures. *Eur J Neurosci* **27:** 2676–2685. doi:10.1111/j.1460-9568.2008.06213.x

Hammer M. 1993. An identified neuron mediates the unconditioned stimulus in associative olfactory learning in honeybees. *Nature* **366:** 59–63. doi:10.1038/366059a0

Hammer M, Menzel R. 1998. Multiple sites of associative odor learning as revealed by local brain microinjections of octopamine in honeybees. *Learn Mem* **5:** 146–156.

Han KA, Millar NS, Davis RL. 1998. A novel octopamine receptor with preferential expression in *Drosophila* mushroom bodies. *J Neurosci* **18:** 3650–3658. doi:10.1523/JNEUROSCI.18-10-03650.1998

Han C, Jan LY, Jan YN. 2011. Enhancer-driven membrane markers for analysis of nonautonomous mechanisms reveal neuron-glia interactions in *Drosophila*. *Proc Natl Acad Sci* **108:** 9673–9678. doi:10.1073/pnas.1106386108

Hayar A, Heyward PM, Heinbockel T, Shipley MT, Ennis M. 2001. Direct excitation of mitral cells via activation of α1-noradrenergic receptors in rat olfactory bulb slices. *J Neurophysiol* **86:** 2173–2182. doi:10.1152/jn.2001.86.5.2173

Honegger KS, Campbell RAA, Turner GC. 2011. Cellular-resolution population imaging reveals robust sparse coding in the *Drosophila* mushroom body. *J Neurosci* **31:** 11772–11785. doi:10.1523/JNEUROSCI.1099-11.2011

Jenett A, Rubin GM, Ngo TTB, Shepherd D, Murphy C, Dionne H, Pfeiffer BD, Cavallaro A, Hall D, Jeter J, et al. 2012. A GAL4-driver line resource for *Drosophila* neurobiology. *Cell Rep* **2:** 991–1001. doi:10.1016/j.celrep.2012.09.011

Jiang M, Griff ER, Ennis M, Zimmer LA, Shipley MT. 1996. Activation of locus coeruleus enhances the responses of olfactory bulb mitral cells to weak olfactory nerve input. *J Neurosci* **16:** 6319–6329. doi:10.1523/JNEUROSCI.16-19-06319.1996

Joerges J, Küttner A, Galizia CG, Menzel R. 1997. Representations of odours and odour mixtures visualized in the honeybee brain. *Nature* **387:** 285–288. doi:10.1038/387285a0

Kaba H, Nakanishi S. 1995. Synaptic mechanisms of olfactory recognition memory. *Rev Neurosci* **6:** 125–142. doi:10.1515/REVNEURO.1995.6.2.125

Karuppudurai T, Lin TY, Ting CY, Pursley R, Melnattur K V, Diao F, White BH, Macpherson LJ, Gallio M, Pohida T, et al. 2014. A hard-wired glutamatergic circuit pools and relays UV signals to mediate spectral preference in *Drosophila*. *Neuron* **81:** 603–615. doi:10.1016/j.neuron.2013.12.010

Kim YC, Lee HG, Lim J, Han KA. 2013. Appetitive learning requires the α1-like octopamine receptor oamb in the *Drosophila* mushroom body neurons. *J Neurosci* **33:** 1672–1677. doi:10.1523/JNEUROSCI.3042-12.2013

Klapoetke NC, Murata Y, Kim SS, Pulver SR, Birdsey-Benson A, Cho YK, Morimoto TK, Chuong AS, Carpenter EJ, Tian Z, et al. 2014. Independent optical excitation of distinct neural populations. *Nat Methods* **11:** 338–346. doi:10.1038/nmeth.2836

Kreher SA, Mathew D, Kim J, Carlson JR. 2008. Translation of sensory input into behavioral output via an olfactory system. *Neuron* **59:** 110–124. doi:10.1016/j.neuron.2008.06.010

Lee T, Luo L. 1999. Mosaic analysis with a repressible neurotechnique cell marker for studies of gene function in neuronal morphogenesis. *Neuron* **22:** 451–461. doi:10.1016/S0896-6273(00)80701-1

Lin AC, Bygrave AM, De Calignon A, Lee T, Miesenböck G. 2014. Sparse, decorrelated odor coding in the mushroom body enhances learned odor discrimination. *Nat Neurosci* **17:** 559–568. doi:10.1038/nn.3660

Linster C, Cleland TA. 2001. How spike synchronization among olfactory neurons can contribute to sensory discrimination. *J Comput Neurosci* **10:** 187–193. doi:10.1023/A:1011221131212

Liu X, Davis RL. 2009. The GABAergic anterior paired lateral neuron suppresses and is suppressed by olfactory learning. *Nat Neurosci* **12:** 53–59. doi:10.1038/nn.2235

Liu C, Plaçais PY, Yamagata N, Pfeiffer BD, Aso Y, Friedrich AB, Siwanowicz I, Rubin GM, Preat T, Tanimoto H. 2012. A subset of dopamine neurons signals reward for odour memory in *Drosophila*. *Nature* **488:** 512–516. doi:10.1038/nature11304

Maqueira B, Chatwin H, Evans PD. 2005. Identification and characterization of a novel family of *Drosophila* β-adrenergic-like octopamine G-protein coupled receptors. *J Neurochem* **94:** 547–560. doi:10.1111/j.1471-4159.2005.03251.x

Masuda-Nakagawa LM, Tanaka NK, O'Kane CJ. 2005. Stereotypic and random patterns of connectivity in the larval mushroom body calyx of *Drosophila*. *Proc Natl Acad Sci* **102:** 19027–19032. doi:10.1073/pnas.0509643102

Masuda-Nakagawa LM, Gendre N, O'Kane CJ, Stocker RF. 2009. Localized olfactory representation in mushroom bodies of *Drosophila* larvae. *Proc Natl Acad Sci* **106:** 10314–10319. doi:10.1073/pnas.0900178106

Masuda-Nakagawa LM, Ito K, Awasaki T, O'Kane CJ. 2014. A single GABAergic neuron mediates feedback of odor-evoked signals in the mushroom body of larval *Drosophila*. *Front Neural Circuits* **8:** 35. doi:10.3389/fncir.2014.00035

Matsumoto Y, Matsumoto CS, Wakuda R, Ichihara S, Mizunami M. 2015. Roles of octopamine and dopamine in appetitive and aversive memory acquisition studied in olfactory conditioning of maxillary palpi extension response in crickets. *Front Behav Neurosci* **9:** 230. doi:10.3389/fnbeh.2015.00230

Menzel R. 2012. The honeybee as a model for understanding the basis of cognition. *Nat Rev Neurosci* **13:** 758–768. doi:10.1038/nrn3357

Monte P, Woodard C, Ayer R, Lilly M, Sun H, Carlson J. 1989. Characterization of the larval olfactory response in *Drosophila* and its genetic basis. *Behav Genet* **19:** 267–283. doi:10.1007/BF01065910

Morita M, Susuki J, Amino H, Yoshiki F, Moizumi S, Kudo Y. 2006. Use of the exogenous *Drosophila* octopamine receptor gene to study Gq-coupled receptor-mediated responses in mammalian neurons. *Neuroscience* **137:** 545–553. doi:10.1016/j.neuroscience.2005.09.012

Nagarkar-Jaiswal S, Lee PT, Campbell ME, Chen K, Anguiano-Zarate S, Gutierrez MC, Busby T, Lin WW, He Y, Schulze KL, et al. 2015. A library of MiMICs allows tagging of genes and reversible, spatial and temporal knockdown of proteins in *Drosophila*. *Elife* **4:** e05338. doi:10.7554/eLife.05338

Nai Q, Dong HW, Hayar A, Linster C, Ennis M. 2009. Noradrenergic regulation of GABAergic inhibition of main olfactory bulb mitral cells varies as a function of concentration and receptor subtype. *J Neurophysiol* **101:** 2472–2484. doi:10.1152/jn.91187.2008

Nern A, Pfeiffer BD, Rubin GM. 2015. Optimized tools for multicolor stochastic labeling reveal diverse stereotyped cell arrangements in the fly visual system. *Proc Natl Acad Sci* **112:** E2967–E2976. doi:10.1073/pnas.1506763112

Nicolaï LJJ, Ramaekers A, Raemaekers T, Drozdzecki A, Mauss AS, Yan J, Landgraf M, Annaert W, Hassan BA. 2010. Genetically encoded dendritic marker sheds light on neuronal connectivity in *Drosophila*. *Proc Natl Acad Sci* **107:** 20553–20558. doi:10.1073/pnas.1010198107

Olshausen BA, Field DJ. 2004. Sparse coding of sensory inputs. *Curr Opin Neurobiol* **14:** 481–487. doi:10.1016/j.conb.2004.07.007

Osumi-Sutherland D, Costa M, Court R, O'Kane CJ. 2014. Virtual fly brain: using OWL to support the mapping and genetic dissection of the *Drosophila* brain. *CEUR Workshop Proc* **1265:** 85–96.

Pauls D, Selcho M, Gendre N, Stocker RF, Thum AS. 2010. *Drosophila* larvae establish appetitive olfactory memories via mushroom body neurons of embryonic origin. *J Neurosci* **30:** 10655–10666. doi:10.1523/JNEUROSCI.1281-10.2010

Perez-Orive J, Mazor O, Turner GC, Cassenaer S, Wilson RI, Laurent G. 2002. Oscillations and sparsening of odor representations in the mushroom body. *Science* **297:** 359–365. doi:10.1126/science.1070502

Pfeiffer BD, Ngo TTB, Hibbard KL, Murphy C, Jenett A, Truman JW, Rubin GM. 2010. Refinement of tools for targeted gene expression in *Drosophila*. *Genetics* **186:** 735–755. doi:10.1534/genetics.110.119917

Poo C, Isaacson JS. 2009. Odor representations in olfactory cortex: 'sparse' coding, global inhibition, and oscillations. *Neuron* **62:** 850–861. doi:10.1016/j.neuron.2009.05.022

Rodrigues V, Siddiqi O. 1978. Genetic analysis of chemosensory pathway. *Proc Indian Acad Sci Sect B Exp Biol* **87:** 147–160. doi:10.1007/BF02837709
Roeder T. 2005. Tyramine and octopamine: ruling behavior and metabolism. *Annu Rev Entomol* **50:** 447–477. doi:10.1146/annurev.ento.50.071803.130404
Roeder T, Seifert M, Kähler C, Gewecke M. 2003. Tyramine and octopamine: antagonistic modulators of behavior and metabolism. *Arch Insect Biochem Physiol* **54:** 1–13. doi:10.1002/arch.10102
Rohwedder A, Wenz NL, Stehle B, Huser A, Yamagata N, Zlatic M, Truman JW, Tanimoto H, Saumweber T, Gerber B, et al. 2016. Four individually identified paired dopamine neurons signal reward in larval *Drosophila*. *Curr Biol* **26:** 661–669. doi:10.1016/j.cub.2016.01.012
Sara SJ, Bouret S. 2012. Orienting and reorienting: the locus coeruleus mediates cognition through arousal. *Neuron* **76:** 130–141. doi:10.1016/j.neuron.2012.09.011
Saumweber T, Rohwedder A, Schleyer M, Eichler K, Chen YC, Aso Y, Cardona A, Eschbach C, Kobler O, Voigt A, et al. 2018. Functional architecture of reward learning in mushroom body extrinsic neurons of larval *Drosophila*. *Nat Commun* **9:** 1104. doi:10.1038/s41467-018-03130-1
Scherer S, Stocker RF, Gerber B. 2003. Olfactory learning in individually assayed *Drosophila* larvae. *Learn Mem* **10:** 217–225. doi:10.1101/lm.57903
Schroll C, Riemensperger T, Bucher D, Ehmer J, Völler T, Erbguth K, Gerber B, Hendel T, Nagel G, Buchner E, et al. 2006. Light-induced activation of distinct modulatory neurons triggers appetitive or aversive learning in *Drosophila* larvae. *Curr Biol* **16:** 1741–1747. doi:10.1016/j.cub.2006.07.023
Schröter U, Malun D, Menzel R. 2007. Innervation pattern of suboesophageal ventral unpaired median neurones in the honeybee brain. *Cell Tissue Res* **327:** 647–667. doi:10.1007/s00441-006-0197-1
Schwaerzel M, Monastirioti M, Scholz H, Friggi-Grelin F, Birman S, Heisenberg M. 2003. Dopamine and octopamine differentiate between aversive and appetitive olfactory memories in *Drosophila*. *J Neurosci* **23:** 10495–10502. doi:10.1523/JNEUROSCI.23-33-10495.2003
Selcho M, Pauls D, Han KA, Stocker RF, Thum AS. 2009. The role of dopamine in *Drosophila* larval classical olfactory conditioning. *PLoS One* **4:** e5897. doi:10.1371/journal.pone.0005897
Selcho M, Pauls D, Huser A, Stocker RF, Thum AS. 2014. Characterization of the octopaminergic and tyraminergic neurons in the central brain of *Drosophila* larvae. *J Comp Neurol* **522:** 3485–3500. doi:10.1002/cne.23616
Sinakevitch I, Mustard JA, Smith BH. 2011. Distribution of the octopamine receptor AmOA1 in the honey bee brain. *PLoS One* **6:** e14536. doi:10.1371/journal.pone.0014536
Slater G, Levy P, Andrew Chan KL, Larsen C. 2015. A central neural pathway controlling odor tracking in *Drosophila*. *J Neurosci* **35:** 1831–1848. doi:10.1523/JNEUROSCI.2331-14.2015
Smith BH, Menzel R. 1989. The use of electromyogram recordings to quantify odourant discrimination in the honey bee, *Apis mellifera*. *J Insect Physiol* **35:** 369–375. doi:10.1016/0022-1910(89)90110-8
Sombati S, Hoyle G. 1984. Central nervous sensitization and dishabituation of reflex action in an insect by the neuromodulator octopamine. *J Neurobiol* **15:** 455–480. doi:10.1002/neu.480150606
Sonnhammer EL, von Heijne G, Krogh A. 1998. A hidden Markov model for predicting transmembrane helices in protein sequences. *Proc AMIA Annu Fall Symp* **6:** 175–182.
Stettler DD, Axel R. 2009. Representations of odor in the piriform cortex. *Neuron* **63:** 854–864. doi:10.1016/j.neuron.2009.09.005
Stevenson PA, Dyakonova V, Rillich J, Schildberger K. 2005. Octopamine and experience-dependent modulation of aggression in crickets. *J Neurosci* **25:** 1431–1441. doi:10.1523/JNEUROSCI.4258-04.2005
Stokes CCA, Isaacson JS. 2010. From dendrite to soma: dynamic routing of inhibition by complementary interneuron microcircuits in olfactory cortex. *Neuron* **67:** 452–465. doi:10.1016/j.neuron.2010.06.029
Stopfer M, Bhagavan S, Smith BH, Laurent G. 1997. Impaired odour discrimination on desynchronization of odour-encoding neural assemblies. *Nature* **390:** 70–74. doi:10.1038/36335
Strother JA, Wu ST, Rogers EM, Eliason JLM, Wong AM, Nern A, Reiser MB. 2018. Behavioral state modulates the on visual motion pathway of *Drosophila*. *Proc Natl Acad Sci* **115:** E102–E111. doi:10.1073/pnas.1703090115
Suver MP, Mamiya A, Dickinson MH. 2012. Octopamine neurons mediate flight-induced modulation of visual processing in *Drosophila*. *Curr Biol* **22:** 2294–2302. doi:10.1016/j.cub.2012.10.034
Tanaka NK, Awasaki T, Shimada T, Ito K. 2004. Integration of chemosensory pathways in the *Drosophila* second-order olfactory centers. *Curr Biol* **14:** 449–457. doi:10.1016/j.cub.2004.03.006
Tao J, Bulgari D, Berkhoudt DA, Calderon MJ, Watkins SC, Velez HJF, Sabeva N, Deitcher DL, Levitan ES. 2019. *Drosophila* Ptp4E regulates vesicular packaging for monoamineneuropeptide co-transmission. *J Cell Sci* **132:** jcs224568. doi:10.1242/jcs.224568
Tomchik SM, Davis RL. 2009. Dynamics of learning-related cAMP signaling and stimulus integration in the *Drosophila* olfactory pathway. *Neuron* **64:** 510–521. doi:10.1016/j.neuron.2009.09.029
Treue S, Martínez Trujillo JC. 1999. Feature-based attention influences motion processing gain in macaque visual cortex. *Nature* **399:** 575–579. doi:10.1038/21176
Turner GC, Bazhenov M, Laurent G. 2008. Olfactory representations by *Drosophila* mushroom body neurons. *J Neurophysiol* **99:** 734–746. doi:10.1152/jn.01283.2007
Venken KJT, Schulze KL, Haelterman NA, Pan H, He Y, Evans-Holm M, Carlson JW, Levis RW, Spradling AC, Hoskins RA, et al. 2011. MiMIC: a highly versatile transposon insertion resource for engineering *Drosophila melanogaster* genes. *Nat Methods* **8:** 737–747. doi:10.1038/nmeth.1662
Wilson DA, Sullivan RM. 2011. Cortical processing of odor objects. *Neuron* **72:** 506–519. doi:10.1016/j.neuron.2011.10.027
Younossi-Hartenstein A, Salvaterra PM, Hartenstein V. 2003. Early development of the *Drosophila* brain: IV. Larval neuropile compartments defined by glial septa. *J Comp Neurol* **455:** 435–450. doi:10.1002/cne.10483
Zars T, Fischer M, Schulz R, Heisenberg M. 2000. Localization of a short-term memory in *Drosophila*. *Science* **288:** 672–675. doi:10.1126/science.288.5466.672

Received June 15, 2020; accepted in revised form October 30, 2020.